Antigen presentation by clonally diverse CXCR5+ B cells to CD4 and CD8 T cells is associated with durable response to immune checkpoint inhibitors.

Authors

Lizhong Ding[1,8,9], Lu Sun[2,8,9], Melissa T. Bu[1,9], Lauren N. Scott [3,9], Robert M. Prins[2,6,7,8,9], Maureen A. Su[4,5,7,8,9], Melissa G. Lechner[3,7,8,9], Willy Hugo[1,7,8,9*]

[1] Department of Medicine, Division of Dermatology,
[2] Department of Neurosurgery,
[3] Department of Medicine, Division of Endocrinology, Diabetes, and Metabolism,
[4] Department of Microbiology, Immunology, and Molecular Genetics,
[5] Department of Pediatrics, Division of Pediatric Endocrinology,
[6] Department of Molecular and Medical Pharmacology,
[7] Jonsson Comprehensive Cancer Center,
[8] Parker Institute for Cancer Immunotherapy,
[9] David Geffen School of Medicine at UCLA, Los Angeles, CA.

Corresponding author:
Willy Hugo[*], Ph.D.: hwilly@mednet.ucla.edu

Abstract

ICI (immune checkpoint inhibitor) induced durable tumor control has been attributed to the activation of cytotoxic T cells expressing high levels of interferon gamma (IFNγ) in the tumor microenvironment (TME). Interestingly, tumors of melanoma patients treated with MAPK pathway inhibitors (MAPKi) also displayed increased infiltration of cytotoxic, IFNγ-secreting T cells. Yet, the rate of durable tumor control after ICI is almost twice that of MAPKi. Our analysis revealed that, while response to ICI and MAPKi both increase intratumoral T cell infiltration and interferon pathway activity, only ICI-responding tumors demonstrate increased infiltration of B cells. Specifically, in response to ICI, CXCR5+ germinal center-like B cells and CXCR5+ follicular helper T (Tfh) cells were recruited by CXCL13-producing, CD8 T cells; *CXCL13* was induced in response to ICI but not MAPKi. These B cells subsequently present antigens to the CD8 T and Tfh cells through the MHC-I and -II pathways, respectively. The T cells then induce B cells' CD40L/CD40 and IFNγ signaling pathways, further enhancing their antigen presentation activity. Accordingly, patients with higher levels of both BCR clonal diversity (allowing more B cell clones to present tumor antigens) and IFNγ signaling activity (suggesting antigen-specific T cell activation) survived significantly longer than those with only either high BCR clonal diversity or IFNγ pathway score. Thus, ICI, but not MAPKi therapy, induces the recruitment of clonally diverse antigen presenting B cells that activate antigen specific Tfh and cytotoxic CD8 T cells to effect a durable antitumor immune response.

Keywords: Melanoma, immunotherapy, checkpoint inhibitors, interferon gamma pathway, T cell, B cell, antigen presentation, antitumor immunity.

Introduction

Metastatic melanoma used to have a dismal median overall survival of only nine months after diagnosis [1, 2]. However, in the last ten years, FDA approved six regimens of immunotherapy and six regimens of targeted therapy against the MAPK pathway and one combination of the two [3, 4]; the majority of which significantly improved the survival of metastatic melanoma patients. Molecular evaluation reveals that melanoma is among the solid tumors with the highest mutational burden [5, 6], which is hypothesized to serve as a source of neoantigens for host immune responses and may predict the response to immunotherapy [7]. The highly immunogenic nature of melanoma have made it the model cancer to study response to immune checkpoint inhibitors (ICI), such as the

blocking antibodies against T cell inhibitory receptors (T cell "checkpoints") CTLA-4 and PD-1 [8, 9, 10, 11]. Despite its remarkable success, clinical response to ICI remains difficult to predict [6, 12, 13, 14]. Previous work highlighted the association of T cell infiltration and patient response to ICI; ICI-treated tumors displayed higher number of infiltrating T cells accompanied by expression of genes related to interferon pathway activities, demonstrating increased production of interferon gamma (IFNγ) of these T cells [15, 16, 17, 18, 19].

On the other hand, the targeting of the MAPK pathway in melanoma started with the discovery of BRAF V600 mutation in about half of all cutaneous melanoma cases, which constitutively activated the pathway's RAF/MEK/ERK signaling [20]. MAPK pathway inhibitor (MAPKi) treatment significantly prolonged the survival of metastatic melanoma patients with BRAF V600 mutation ($BRAF^{V600}$ mutant melanoma) [21, 22, 23]. In addition to its direct tumor suppressive effect through MAPK pathway inhibition, MAPKi treatment also increases the infiltration of antitumor T cells into the tumor microenvironment (TME) [24, 25].

Intriguingly, the 5-year survival rate of $BRAF^{V600}$ mutant melanoma patients treated with MAPKi is only around half that of ICI (34% after combined therapy using BRAF and MEK inhibitors vs. 60% after combined PD-1 and CTLA-4 antibodies) despite a similar rate of initial response (MAPKi: 68% vs ICI: 58%) [11, 26, 27]. It is worth noting that a separate analysis of another cohort treated with two different BRAF and MEK inhibitors showed a similar 5-year survival rate (31%) that is around half of ICI [33]. Despite the potential differences among the patient cohorts, such large differences in survival between ICI and MAPKi treated melanoma suggest that immune response induced by ICI were more effective than MAPKi to produce durable suppression of the tumor. Indeed, a matching-adjusted study comparing ICI and MAPKi indicated that ICI treatment improved overall survival (OS) of BRAF-mutant melanoma patients when compared to MAPKi [28].

In this study, we aim to discover changes in gene expression and immune factors that are significantly associated with enhanced survival of melanoma patients after ICI treatment. Instead of focusing on identifying patients who will likely respond to ICI from the profiles of their pre-treatment (PT) biopsies, we focus on understanding the profiles from on-treatment (OT) tumors of patients responding to ICI. Based on such profiles, we can identify the immune populations/pathways that are uniquely associated with response to ICI and propose therapeutic strategies to enhance these populations and improve the rate ICI response in patients. Previous work compared the on-treatment tumors of patients responding to ICI (ICI OT-R) compared with those from patients not responding to ICI (ICI OT-NR). However, this comparison is not necessarily informative since ICI OT-NR tumors generally have less immune infiltration compared to ICI OT-R and most immune cell-related markers were upregulated in ICI OT-R group. Which of these are drivers of ICI's durable response vs. insignificant bystanders is therefore unclear.

Here, we applied a novel comparative analysis between melanoma treated with ICI [18, 29] vs. MAPKi [25, 30, 31]. Given that the immune infiltration associated with MAPKi is relatively ineffective, this comparison allowed us to separate drivers of durable response from immune "bystanders" in ICI OT-R. Since MAPKi OT-R tumors also have more immune infiltration than MAPKi OT-NR tumors, yet MAPKi OT-R patients are less likely to achieve a durable response than ICI OT-R patients, we posit that immune genes/pathways that are upregulated/enriched in ICI OT-R, but not in MAPKi OT-R tumors, can help explain the higher rate of durable responses in ICI treated patients. Our comparative analysis highlighted upregulation of *IFNG* transcript expression and the activation of interferon gamma pathway in both ICI OT-R and MAPKi OT-R tumors as previously published [15, 16, 17, 18, 19, 24, 25]. However, we discovered upregulation of *CXCL13* expression of *PDCD1*+ *TOX*+ CD8 T cells only ICI OT-R tumors, relative to MAPKi OT-R tumors; this *CXCL13*+ *PDCD1*+ *TOX*+CD8 T cell population was shown to be tumor-reactive cytotoxic CD 8 T cells [32]. The upregulation of *CXCL13* is associated with higher infiltration of *CXCR5*+ B cells and *CXCR5*+ follicular helper CD4 T cells (Tfh). This interaction strongly suggests the formation of tertiary lymphoid structures (TLS) in the TME, which was reported to be enriched in ICI-OT R tumors [33, 34 35, 36].

Our integrated analysis reveals interactions between the B cells, acting as antigen presenting cells (APC), and both Tfh and CD8 T cells in the TME. Successful presentation of tumor antigens resulted in activation of the T cells, resulting in secretion of IFNγ by CD8 T cells (and, presumably, increased tumor killing activities) and up-expression of CD40L by Tfh cells. The increased expression of CD40L and IFNγ is expected to enhance the antigen presentation activity of the B cells. Importantly, higher BCR diversity, which is expected to increase the chance of tumor antigen uptake and presentation to T cells, is significantly correlated with patient survival after ICI therapy across multiple independent melanoma cohorts. On the other hand, higher BCR clonality was not associated with improved survival after ICI, suggesting that B cells' clonal expansion and specific antibody production are less correlated with response to ICI.

Finally, we demonstrated that BCR diversity and IFNγ signaling pathway scores are significant variables that are correlated with survival after ICI therapy. Patients whose tumors display both higher BCR clonal diversity and interferon pathway activity after ICI have significantly longer survival than those with only higher B cell diversity or IFNγ signaling pathway activity. Intriguingly, there is a hint of synergistic dependence between the two variables; this dependency supports the premise that both clonally diverse antigen presenting B cells and successful antigen presentation to CD8 T cells (as indicated by the IFNγ signaling activation) are needed for an optimal antitumor T cell response after ICI. Our results also strongly suggest a combination of ICI with therapies that enhance antigen presentation by clonally diverse B cells can result in a more durable antitumor immune response in patients.

Results

ICI and MAPKi treatment both induce comparable levels of T cell infiltration but ICI induces a more cytotoxic T cell phenotype.

In order to perform a comparative analysis of transcriptomic response to ICI and MAPKi, we analyzed two separate immunotherapy datasets [18, 28] and three targeted therapy datasets [25, 30, 31] (Supp. Fig 1A, Supp. Table 1A). All samples were classified into three groups: pre-treatment (PT), on-treatment responding (OT-R), and on-treatment non-responding (OT-NR). OT-R is defined by clinical benefit after therapy (CR, PR, or SD by RECIST criteria). OT-NR is defined by no clinical benefit (PD) (Supp. Table 1A). Gene expressions in samples across the datasets were integrated and batch normalized (Supp. Table 1B, see Methods).

We asked whether the differentially expressed genes (DEGs) between ICI and MAPKi could reveal any cell populations or processes that may explain ICI's more durable antitumor response. To this end, we selected the genes that are relatively upregulated in the OT-R compared to the OT-NR samples of each therapy (Fig 1A, see Methods for details). The genes were grouped into either ICI-specific, MAPKi-specific, or ICI and MAPKi-shared DEGs (Fig 1B, Supp. Table 1C). Gene sets that were enriched by these DEGs were computed using Enrichr [37].

We first noted gene sets related to T cells being enriched in the OT-R groups of both therapies (Fig 1C, Supp. Table 1D). Multiple studies had highlighted the importance of increased T cell infiltration and activities for ICI response [15, 17, 19, 29, 38]. The levels of general T cell marker (*CD3D*), cytotoxic CD8 T cells (*CD8B*) and T cell signature were significantly higher in the OT-R tumors of MAPKi or ICI compared to PT and OT-NR tumors (Fig 1D, Supp. Fig 1B, Supp. Table 1E). The magnitude of increased T cell marker expression in the OT-R samples was not different between ICI and MAPKi in either PT, OT-R or OT-NR samples (Supp. Fig 1C). We then asked whether there were differences in the activity of these infiltrating T cells. The total expression of *IFNG*, *GZMB*, and *PRF1* were higher in ICI OT-R than MAPKi OT-R (Fig 1E; *PRF1* is higher in ICI OT-R but not statistically significant), implying that the T cells were more activated and more cytotoxic in response to ICI. Another measure of an effective antitumor T cell activity is the activation of the IFNγ signaling pathway (for brevity, we will refer to IFNγ signaling pathway as IFNγ pathway). Increased of IFNγ pathway score was observed in response to either therapy but the magnitude of the increase was not different between ICI and MAPKi (Fig 1F, Supp. Table 1F).

We further estimated the level of activity on a per T cell basis by computing the ratio between normalized expression of T cell activity markers and *CD8B;* this ratio approximates the average expression of the activity markers per CD8 T cells. On this approximated per-CD8 basis, we observed that *IFNG* did not change significantly in response to either ICI or MAPKi while (Supp. Fig 1D). On the other hand, *CD8B*-normalized expression of the cytotoxic genes *GZMB* and *PRF1* were significantly lower after MAPKi (Fig 1G). Overall, our analysis demonstrated a less cytotoxic CD8 T cells after MAPKi treatment as compared to ICI.

Differences in the cytotoxicity of the T cells seems to affect patient survival. Higher normalized expression of CD8 T cell marker *CD8B* or higher IFNγ gene set enrichments in the ICI OT tumors was significantly correlated with longer OS (Fig 1H). The correlation was not observed in MAPKi OT tumors. Of note, the MAPKi RNA-seq datasets only provided progression free survival (PFS) information. We confirmed that melanoma patients' PFS after MAPKi is significantly correlated with their OS in another MAPKi treated microarray datasets with both PFS and OS information [39, 40] (Supp. Fig 1E, Supp. Table 2). Neither *CD8B* expression nor IFNγ pathway score in PT biopsies was not significantly correlated with survival (Supp. Fig 1F).
Thus, in contrast to MAPKi, T cell infiltration and antitumor cytotoxicity in response to ICI is associated with longer patient survival.

B cells were more abundant in ICI OT tumors and were correlated with improved survival after ICI therapy.

To objectively parse other potential mechanisms underlying ICI-enhanced T cell cytotoxicity, we next examined the DEGs that are upregulated more in ICI OT-R tumors (with respect to ICI OT-NR) than in MAPKi OT-R tumors (with respect to MAPKi OT-NR). For each gene, we directly subtracted its log fold change between OT-R vs. OT-NR samples of ICI and MAPKi-treated tumor samples. We observed a gene set related to CD19+ B cells (Fig 1C) and B cells and DC (Fig 2A, Supp. Table 1D) were upregulated higher in ICI OT-R tumors. On the other hand, MAPKi OT-R tumors showed enrichment of non-immune related gene sets such as neuron, melanocyte and adipocyte related genes (Supp. Fig 2A, Supp. Table 1D).

The expressions of B cell gene markers, B cell signature and immunoglobulin genes were higher in ICI OT-R tumors, when compared to the ICI OT-NR and ICI PT tumors (Fig 2B, Supp. Fig 2B, Supp. Table 1E). In the two ICI datasets that we analyze, B cell marker expression was significantly higher only in the OT but not PT tumors of patients benefiting from ICI (Supp. Fig 2C); this implies that the level of intratumoral B cells pre-therapy is a relatively weak predictor of ICI response. Upregulation of B cell markers and signatures were also observed in MAPKi OT-R tumors, compared to the MAPKi OT-NR tumors, but the differences were less than that of ICI (Fig 2B, Supp. Fig 2B).

The presence of tertiary lymphoid structures (TLS) has been correlated with improved survival after ICI therapy in melanoma [33, 34] and other cancers [35, 36]. We noted that both ICI and MAPKi treatment increased the scores of two recently reported TLS signatures [37] with ICI inducing a more significant increase (Supp. Fig 2D, Supp. Table 1F). Importantly, the expression of TLS-associated, germinal center B cell (GC B cells) and follicular helper T cell (Tfh) markers, *CXCR5* and *BCL6*, were significantly upregulated only in response to ICI but not MAPKi (Fig 2C). Among the differentially expressed of immune related cytokines and chemokines, the expression of *CXCL13*, which is the ligand for *CXCR5*, were significantly increased only in ICI OT-R samples (Fig 2D). The upregulation and higher absolute expression of *CXCL13* after ICI treatment is expected to recruit *CXCR5*+ B cells and *CXCR5*+ Tfh cells. Another chemokine that are upregulated higher in ICI treated tumors is *CCL21*, which is expressed by lymphatic endothelial cells and reticular stromal cells in lymphoid organs [41] and is essential for the trafficking of *CCR7*+ naïve/memory T cells, B cells or activated DCs into secondary lymphoid organs.

Importantly, the expression of B cell marker, *CD19*, or the TLS signature score significantly correlated with survival after ICI therapy but not MAPKi (Fig 2E). However, the level of B cell marker or the TLS signature in the PT samples is not associated with survival (Supp. Fig 2E) other than a trend toward positive association between the TLS signature in MAPKi PT tumors and survival. In all, response to ICI is marked with increased expression of B cell markers, accompanied with markers (*CXCR5*, *BCL6*), gene signatures and secreted factors (*CXCL13*, *CCL21*) that are indicative of TLS formation in the TME.

Enrichment of B cell and TLS gene markers in single cell transcriptome of ICI-treated melanoma

To corroborate our observations in the bulk RNA-seq data at a single cell level, we analyzed a published single cell RNA-seq (scRNA-seq) dataset of ICI-treated melanoma [38]. After normalization and scaling of the gene expression values (see Methods), we re-clustered the single cells and identified the cell types based on differentially upregulated immune gene markers in each cluster (Fig 3A, B, C, Supp. Table 3A). Clusters of known immune populations, such as memory T cells (*CD4/8+ CCR7+ TCF7+*), activated CD8 T cell (*IFNG+* or high in interferon downstream genes (ISGs)), activated/exhausted CD8 T cell (*PDCD1+ CTLA4+ TOX+*) with high expression of *CXCL13*, B cell (*CD19+ MS4A1+*), plasma cell (*SDC1+ IGHG/A+*), NK cells (*FCGR3A+ GNLY+*), Tregs (*FOXP3+ CTLA4+*), monocyte/ macrophage (*CD14+ CD163+*), monocyte-derived dendritic cells (mono DC: *CD14+ CLEC10A+*), plasmacytoid DC (*LILRA4+*) and proliferating cells (*MKI67+*), were marked accordingly. We further identified a subset of *PDCD1+ CXCL13+ CTLA4+ TOX+ TCF7+ CD4+* T cells, which also expressed *CXCR5* and *BCL6* (Fig 3B); this potentially is a population of activated *CXCR5+ CXCL13+* follicular helper T cells (Tfh). We also noted the expression of *BCL6* and *REL* in the B cell population (Fig 3C); along with *BCL6*, *REL* is a transcription factor that is upregulated in GC B cells [42].

As the scRNA-seq is done on the CD45+ fraction of the tumor (i.e intratumoral immune cells), we could ask whether the proportions (but not absolute numbers) of each cell population were different in the responder vs. non-responder to ICI. Corroborating the B cell marker up-expression in ICI OT-R tumors in bulk RNA-seq, we noted a significantly increased proportion of B cells in ICI OT-R samples compared to OT-NR samples (Fig 3D, red boxplots, bottom, Supp. Table 3B). We also noted that the proportion of B cells was already higher in the PT-R samples (Fig 3D, red boxplots, top, Supp. Table 3B), but, as we will show later, B cell clones infiltrating the pre- and post-ICI tumors are largely non-overlapping. Importantly, B cell abundance in the ICI OT tumors was significantly correlated with the patients' improved OS (C).

Looking at the other cell populations, the proportion of *CCR7+ TCF7+* memory T cells per sample were higher in the PT-R and OT-R samples (Fig 3D, leftmost violet boxplot, Supp. Table 3B), in line with the original publication [38]. One population with significantly higher proportion in the PT-NR and OT-NR biopsies is the proliferating cluster (Supp. Table 3A, rightmost dark blue cluster), which showed high expression of *CD3D*, *CD8A*, *PDCD1*, *CTLA4* and *TOX* (Fig 3B, last boxplot). A similar population of proliferative CD8 T cells expressing multiple T cell exhaustion marker was previously reported to be an intermediate exhausted cytotoxic T cells; they are expected to differentiate into terminally exhausted T cells [43]. There is a trend of higher proportion of CD14+ CD163+ monocyte/macrophage (Mφ) population in the ICI OT-NR tumors (Supp. Fig 3A, purple boxplot), and a higher proportion of this population was associated worse OS after ICI (Supp. Fig 3B).

In each cell population, we analyzed the genes that are increased in expression in ICI OT-R tumors when compared to OT-NR tumors (Supp. Table 3D). Agreeing with the observation of increased GC B cells in response to ICI, we observed significant upregulation of *BCL6* and *REL* in the CXCR5+ B cell population (Fig 3F). We also confirmed that the expression of *CXCR5* was significantly increased in Tfh/Tph population (Fig 3F, green boxplots), implying a higher proportion of Tfh cells in ICI OT-R tumors. The scRNA-seq data allows us to trace

the source of *CXCL13* expression in the ICI OT-R vs. OT-NR tumors; *CXCL13* was significantly upregulated in the *PDCD1*+ *TOX*+ CD8 T cell in ICI OT-R tumors, while it was upregulated in the Tfh population of the OT-NR tumors (Fig 3G, top). Of note, *CXCL13*+ *PD1*+ *TOX*+ CD8 T cell population was recently reported to comprise a high fraction of tumor antigen-specific CD8 T cells that are dysfunctional/exhausted [32].

Supporting this premise, receptor-ligand interaction analysis using CellChat predicted that *CXCL13* expressed by *PD1*+ *TOX*+ CD8 T cells (source) engaged CXCR5+ B cells (target) (Fig 3H). On the other hand, ICI OT-NR tumors show a mixture of CXCL16-CXCR6 and CXCL13-CXCR3[44] interaction among the monocytic DC, macrophages and T cells (with weak CXCL13-CXCR5 interaction involving B cells) (Fig 3H). Although the relative fractions and normalized expression of *CXCL13* and *CXCR5* were similar between ICI OT-R and OT-NR (Fig 3H, dot plots), the CXCL13-CXCR5 interaction is expected to be stronger in ICI OT-R group since there was a larger fraction of CXCR5+ B cells within the CD45+ immune cells of the latter. Finally, AUCell analysis [45] using showed enrichments of TLS gene sets specifically in B and Tfh cell clusters (Supp. Fig 3C), indicative of TLS formation within which CD8+ T, CD4+ Tfh and GC B cells are interacting. Overall, ICI-mediated release of T cell checkpoint engagement of tumor-specific, PD1+ TOX+ CD8 T cells may upregulate CXCL13, which subsequently recruits CXCR5+ B cells and Tfh to form TLS in the TME.

Response to ICI is associated with antigen presentation activity of intratumoral B cells.

In line with its role as antigen presenting cells (APCs), one of the most enriched receptor-ligand interactions involving the B cells was the MHC class II pathway (Supp. Fig 4A). Notably, B cells were predicted to present antigens to the *CXCR5*+ *CXCL13*+ Tfh only in the ICI OT-R tumors (Fig 4A). In OT-NR tumors, MHC II interaction was dominated by those between MHC II+ cells and the CD4+ Tregs. Antigen recognition by Tfh result in the activation their T helper function, which provides stimulatory signal CD40+ B cells through upregulation of CD40L [46, 47, 48]. Indeed, we observed the upregulation of *CD40LG* transcript in ICI OT-R tumors (Fig 4B, Supp. Table 3D), which suggests a productive antigen presentation by the B cells to the Tfh. On the B cells, we observed upregulation of the APC maturation marker, *CD83*, which is upregulated upon BCR ligation and CD40/CD40L pathway activation [49] (Fig 4B, Supp. Table 3D). Receptor-ligand interaction analysis on the genes in CD40 pathway showed enrichment of the pathway only in the ICI OT-R tumors (Fig 4C, Supp. Fig 4A). Curiously, MHC I pathway related interaction was dominated by that between B cells and the *CXCL13*+ *PD1*+ *TOX*+ CD8 T cells, hinting cross-presentation of tumor antigens through MHC I presentation (Supp. Fig 4B). CD40L and IFNγ-driven activation of B cells was recently shown to induce antigen cross presentation in B cells [50] and both factors are shown to be abundant in the TME of ICI OT-R tumors.

Using their B cell receptor (BCR), B cells can selectively capture tumor-specific antigens and present them to Tfh cells [51]. We surmise that, if the B cells are presenting tumor antigens to Tfh through BCR-driven internalization of extracellular tumor antigens, then a more diverse BCR repertoire should improve the chance of a successful antigen presentation. To obtain an estimate of the B cells' clonal dynamics, we applied TRUST4 on both bulk RNA-seq and scRNA-seq reads [52]. We assigned each B cell's clonal identity by its IGH chain's CDR3 sequence. Response to ICI exhibited statistically significant increase of BCR diversity in ICI OT-R tumors (with respect to both PT and OT-NR); MAPKi OT-R tumors showed a similar albeit much weaker trend (Fig 4D, Supp. Table 1G). Using SCOPer [53], we observed an indication of increased somatic hypermutation (SHM) in ICI OT-R tumors; this may have contributed to the increase of BCR diversity in ICI OT-R tumors (Fig 4E). Interestingly, the trend is somewhat reversed with BCR clonality, ICI OT-R tumors did not have a higher BCR clonality than ICI PT or OT-NR tumors while MAPKi OT-R tumors did (Fig 4D, Supp. Table 1G). This suggests that MAPKi therapy induces a different B cell phenotype from ICI. In fact, tumor associated B cells were implicated in the development of MAPKi resistance [54], suggesting that MAPKi-induced B cell to be more immunosuppressive.

Examining the correlation of BCR clonal pattern with survival, we noted that BCR diversity was associated with improved survival after ICI but not MAPKi therapy (Fig 4F). Strikingly, the significant correlation between BCR diversity, but not BCR clonality, and the patient's OS held in both the bulk RNA-seq and scRNA-seq cohorts (Fig 4F, G, Supp. Table 3E, Supp. Table 4A). Although previous studies highlighted the prognostic significance of higher B cell fraction and TLS detection frequency in the PT-R tumors [33, 34], we observed that most B cell clones in the ICI OT-R tumors were newly infiltrating clones after the therapy (Supp. Fig 4C) The same predominance of OT tumor specific clones can also be observed in the T cell populations (Supp. Fig 4D). The clonal dynamics of both the T and B cells after ICI treatment curiously matches the "T cell clonal replacement" reported in basal/squamous cell carcinomas that responded to ICI; most of the ICI-induced tumor infiltrating T cells were novel T cell clones not observed in the PT tumors of the same patient [29, 55]. However, only BCR but not TCR diversity was correlated with the patients' OS (Supp. Table 4A).

Compared to ICI, the increase in B cell infiltration and BCR diversity between MAPKi OT-R and OT-NR samples were significantly smaller. Both B cell clonality and diversity were not associated with improved survival after MAPKi therapy. These observations strongly hint that the B cells' role in ICI response is to present T cells with a broad variety of tumor antigens by highly diversified intratumoral B cell clones rather than to generate tumor specific antibodies through their differentiation into plasma cells.

Concomitant increase in B cell clonal diversity and IFNγ pathway activity correlates with significantly longer survival after ICI.

ICI-mediated reprieve of the suppressive T cell checkpoint and, presumably, antigen recognition by CD8 T cells induced IFNγ expression in the ICI OT-R TME (Fig 1G). IFNγ expression by *PDCD1+ TOX+*, *IFNG+* and *MKI67+* CD8 T cells was predicted to activate the IFNγ pathway in B cell and monocytic DC in ICI OT-R tumors (Fig 5A). On the other hand, IFNγ pathway was activated mainly in the monocytic DC and *CD14+ CD163+* macrophage population. The activation of IFNγ pathway in B cells of ICI OT-R tumors is expected further boost their antigen presentation activity, resulting in additional activation of the Tfh and CD8 T cells.

When stratified by the enrichment of hallmark interferon gamma gene set and BCR diversity of their tumors (high: median and above, and, low: below median), ICI-treated patients with the best survival were those with high hallmark interferon gamma gene set and BCR diversity in their OT samples (Fig 5B, log-rank P=0.0072). Cox proportional hazard analyses suggested that hallmark interferon gamma gene set score and BCR diversity in the OT samples are independent predictors of survival in ICI treated patients (Fig 5C, Supp. Table 4B). Stratification of the patients by the expression of CD8 T cell marker *CD8B* and B cell marker *CD19* show a similar trend where patients with high expression of both *CD19* and *CD8B* had better survival after ICI treatment (Supp. Fig 5A), in agreement with a recent report on a separate cohort of melanoma patients [34]. Curiously, our analysis also revealed an interaction/dependency between BCR diversity and hallmark interferon gamma gene set scores in relation with the patients' OS (Supp. Fig 5B, Supp. Table 4C, HR of interaction = 0.55, P = 0.054), which suggests that successful antigen presentation by B cells to the T cells, resulting in an increased IFNγ pathway activity in the TME, is crucial for ICI response.

Discussion

To discover immune factors and pathways associated with durable response to ICI-based immunotherapy, we analyzed the transcriptomic profiles of melanoma biopsies taken before and after ICI treatment. Unique to our study is the utilization of transcriptomic profiles of melanoma biopsied pre- and post-MAPKi therapy to filter out immune-related gene expression changes that are less/not associated with a durable antitumor immune response

(the "bystander" immune response). Genes that are upregulated only in ICI OT-R tumors highlighted enrichment of B cell and Tfh markers, strongly hinting at the presence of TLS in the tumor. Indeed, increased presence of TLS has been correlated with ICI response in multiple cancer histologies [33, 34, 35, 36].

We demonstrated that the increase of TLS-associated CXCR5+ B cells and Tfh is correlated with increased mRNA expression of CXCR5's ligand, CXCL13; this was reported previously [57]. We further narrowed down the source of *CXCL13* upregulation in ICI OT-R tumors to be the population of activated/exhausted, tumor reactive CD8 T cells [32, 56]. We propose a model where response to ICI is marked with CXCL13+ CD8 T cell-driven recruitment of highly diversified, CXCR5+ B cell clones, whose (tumor) antigen presentation activities induce and sustain the activation of tumor-reactive CD4 Tfh and CD8 T cells (Fig 5D).

Importantly, our results suggest that B cells mainly function as APCs in ICI OT-R tumors. First, our cell-cell interaction analysis highlighted CXCR5+ B cells as the dominant antigen presenting cells in ICI OT-R TME, presenting antigens to both CD8+ tumor-reactive T cells and CD4+ Tfh cells and through MHC I and MHC II pathways, respectively. We observed a concomitant overexpression of *CD40LG* in the Tfh population and reflecting a productive antigen presentation by the B cells to the Tfh [51, 58]. CD40L up-expression on the Tfh in turn activated the CD40 pathway in the B cells, as shown by upregulation of *CD83* [49]. Notably, CD83 is a marker of light zone-specific, antigen presenting GC B cells [46, 59] and its expression is crucial for B cell longevity after antigen stimulation [60]. Overall upregulation of *IFNG* expression in ICI OT-R tumors (bulk RNA-seq) was predicted to significantly activate the IFNγ pathway of the B cells in ICI OT-R tumors. Simultaneous activation of IFNγ and CD40 signaling pathways in B cells can increase B cell's antigen cross presentation activity to CD8 T cells [50, 61]. Successful cross-presentation is expected to induce further activation of tumor antigen-specific CD8 T cells, resulting in a strong cytotoxic activity against the tumor.

Another orthogonal support to B cells' APC role in ICI response came from the clonal dynamis of B cells in ICI OT-R tumors. Through a computational reconstruction of BCR sequences from the RNA-seq data, we discovered significant correlation between BCR diversity in ICI OT tumors, but not BCR clonality, and OS after ICI therapy. Indeed, higher BCR diversity should lead to a better chance of some clones successfully presenting antigens to T cells. The absence of association between BCR clonality and OS indicated that the subsequent differentiation and clonal expansion of B cells to antibody producing plasma cells is less essential to ICI-induced long-term antitumor immunity in melanoma, further supporting these B cells' function as APC. Notably, the association with BCR diversity and no-association with BCR clonality were confirmed both in the bulk RNA-seq and scRNA-seq ICI datasets. Finally, we demonstrated that higher BCR diversity and IFNγ pathway score were synergistically associated with longer OS after ICI.

Our study has several limitations. First, it is a correlative, retrospective study of combined cohorts of ICI-treated tumors. We ensured that our initial observations in the RNA-seq cohorts are corroborated in the independent scRNA-seq cohort. For instance, the association of B cell abundance and BCR diversity with improved OS after ICI were confirmed in both bulk RNA-seq and scRNA-seq cohorts. Importantly, our bulk RNA-seq-derived observation of synergistic interaction between BCR diversity and IFNγ pathway activity in predicting survival after ICI also corroborated the cell-cell interaction analysis of the scRNA-seq. Importantly, there are multiple pre-clinical studies showing the importance of antigen specific, T cell-B cell interaction in ICI response [51, 62, 63]. Another limitation is that the use of RNA-seq to reconstruct the CDR3 regions of the TCR or BCR may have limited sensitivity. Again, we tried to limit our claims to the observations that were supported by both the bulk and scRNA-seq data. Additional studies using direct TCR/BCR sequencing of ICI-treated tumors will be needed to confirm our observations.

Our results demonstrate that an effective immune response to ICI involves activation of tumor-reactive CD4 and CD8 T cells by antigen presenting B cells, likely in the context of TLS in the TME. Thus, the next logical

question is how to leverage this observation in the clinic. Several studies have attempted direct TLS formation using TLS-associated secreted factors [64, 65, 66, 67], most notably, CXCL13 [68, 69]. However, TLS formation may not be sufficient to ensure successful B cell and T cell activation [70]. Strategies to pre-load tumor antigens on B cells to generate B cell vaccine, just like DC vaccine [71], may be more promising in the context of combinatorial therapy with ICI. B cell-based neoantigen vaccines was reported to promote ICI efficacy in animal models of lung cancer [51] and GBM [50, 51]. There is a need for additional pre-clinical and, ultimately, clinical studies to systematically test the most optimal B cell-vaccine approach to enhance the rate of durable ICI response.

Methods

Datasets used. In order to perform a comparative analysis on transcriptomic response to ICI and MAPKi, we analyzed two batches of immunotherapy data and two batches of targeted therapy data. The two immunotherapy datasets are from Riaz N, et al. [29] (named 2017_Cell_NR) and Abril-Rodriguez G, et al. [18] (named 2020_NC_GA). The patients of these two cohorts were treated with antibodies against the PD-1 receptor (anti-PD-1) including nivolumab and pembrolizumab. The two targeted therapy datasets are derived from Hugo W, et al. [25, 30] (named 2015_Cell_WH) and from Kwong LN, et al. [31] (named 2015_JCI_LK). These patients were treated with either BRAF inhibitor monotherapy or BRAF and MEK inhibitors combination therapy (BRAFi: vemurafenib, dabrafenib, encorafenib; MEKi: cobimetinib, trametinib, binimetinib; one patient was treated with trametinib monotherapy). All samples were classified into three groups: pre-treatment (PT), on-treatment responding (OT-R), and on-treatment non-responding (OT-NR). OT-R is defined by clinical benefit after therapy (CR, PR, or SD by RECIST criteria). OT-NR is defined by no clinical benefit (PD) (Supp. Table 1A). For single cell transcriptome analysis, we utilized the data from Sade-Feldman et al [38]. The data profiled 16,291 immune cells (CD45+ cells) from 48 tumor samples of melanoma patients treated with ICI. All samples were classified into four groups: pre-treatment responding (PT-R), pre-treatment non-responding (PT-NR), on-treatment responding (OT-R), and on-treatment non-responding (OT-NR). The PFS and OS data of MAPKi treated patients (Supp. Table 2) were extracted from two separate publications; both studies were not incorporated in our combined analysis as they only provide microarray datasets [39, 40].

Gene expression analysis. The bulk RNA-seq data was re-aligned to hg38 human reference genome using HiSAT2 (v2.1.0), then processed using samtools (v1.10) and picard (v2.25.0). The gene expression count was calculated using htseq-count (v0.11.2). The gene expression was normalized using trimmed mean of M-values (TMM) and converted to count per million (cpm) expression value using edgeR R package (v3.32.1). Batch effect was corrected using removeBatchEffect function in the R package limma (v3.46.0). The normalized expression of each gene (in $\log_2$ cpm) is provided in Supp. Table 1B.

Differential gene expression analysis. We first computed the expression change of each gene (in $\log_2$ FC) between the PT and OT samples of each patient (the OT samples can be OT-R or OT-NR). Thus, each gene will have a list of $\log_2$ FC values associated with therapy response (OT-R with respect to their respective PT) and resistance/non-response (OT-NR w.r.t their respective PT). Differentially expressed genes (DEGs) between the OT-R and OT-NR groups were defined by:

1) two-fold difference between the arithmetic average of $\log_2$ FCs in OT-R and arithmetic average of $\log_2$ FCs in OT-NR ($\Delta\log_2 FC \geq 1$ where $\Delta\log_2 FC = \text{mean}(\log_2 FC(OT\text{-}R)) - \text{mean}(\log_2 FC(OT\text{-}NR))$), and,
2) FDR-adjusted t-test p value < 0.05 between the $\log_2$ FCs of the OT-R and OT-NR groups.

The sets of DEGs that are upregulated in the OT-R groups of either therapy were shown in Fig 3A. The gene sets/ontologies that are enriched in the ICI-specific, MAPKi-specific and ICI and MAPKi shared DEGs were computed using Enrichr [37] (see the **gene set analysis** section). Other than comparing the list of DEGs, we also directly computed the difference of $\log_2$ FC difference between the OT-R and OT-NR groups across the two therapies. For instance, to find the genes that are upregulated at least two-fold higher in ICI's responder when compared to MAPKi responders (after adjusting with their respective non-responder groups), we selected genes

satisfying:

1) $\Delta\Delta FC_{ICI\text{-}MAPKi} \geq 1$, where $\Delta\Delta FC_{ICI\text{-}MAPKi} = \Delta\log_2 FC_{ICI} - \Delta\log_2 FC_{MAPKi}$, and,
2) $\Delta\log_2 FC_{ICI} \geq 1$

Conversely, the genes that are upregulated in MAPKi's responder were computed in the same manner. The shortlisted genes were also analyzed for gene set enrichment using Enrichr. The results are in Supp. Table 1C, D.

Gene sets analysis. In this study, we used the interferon gene sets from the Molecular Signatures Database (MSigDB) [72, 73]. Specifically, we collected gene sets containing the keyword "IFN" or "interferon" from the H: hallmark gene sets, C2 CGP: chemical and genetic perturbations, C6: oncogenic signatures, and C7: immunologic signatures (Supp. Table 1F). The gene set of TLS signatures were manually curated in gmt file format. Cabrita *et al* developed two gene sets that reflected the presence of TLS in melanoma. One TLS signature of nine genes (*CD79B, CD1D, CCR6, LAT, SKAP1, CETP, EIF1AY, RBP5, PTGDS*) were found using differential expression analysis. The other TLS signature of seven genes (*CCL19, CCL21, CXCL13, CCR7, CXCR5, SELL, LAMP3*) were constructed from a compendium of TLS hallmark genes [34]. Gene Set Variation Analysis (GSVA) [74] was used to calculate single sample gene set enrichment scores, using the R packages GSVA (v1.38.2), GSVAdata (v1.26.0), and GSEABase (v1.52.1).

Clonotype analysis. As for the TCR clonotyping, the raw output of clonotypes was derived from the raw FASTQ reads of the bulk RNA-seq data using TRUST4 (v1.0.4) with default settings. Nonproductive CDR3aa were removed the raw output. Clonotypes are separated by chain names such as TRA, TRB, TRD, TRG, IGH, IGK, IGL. Convergent clonotypes, which possess the same amino acid sequences but different nucleotide sequences, were merged. As for the BCR clonotyping, considering the SHM mechanism of GC B cells, productive IGH chains were selected from the raw AIRR standard format [75] output derived from the bulk RNA-seq data using TRUST4 (v1.0.4). Then the hierarchicalClones() function in the R package SCOPer [53] (v1.2.0) was used to infer—based on the nucleotide sequence—the germline BCR clones that arise from V(D)J recombination (in the bone marrow) [76][75] and mature (SHM-generated) BCR clones that are derived from germline clones after somatic hypermutation process in the germinal center [42]. The R package SHazaM [77] (v1.1.0) was used to automatically calculate the threshold for the bimodal distribution in the hierarchicalClones() function as defined by the SCOPer pipeline. Consequently, the SHM occurrence frequency can be calculated using the count of germline clones associated with more than one mature BCR clone divided by total count of the germline clones. The clonotype repertoire metrics of TCR and BCR, including count, diversity and clonality were calculated using the custom R package rTCRBCRr (v0.1.0) and other custom R scripts.

Cell population abundance estimation. The R package MCPcounter (v1.2.0) was applied to the normalized $\log_2$ cpm expression matrix from the bulk RNA-seq data in order to estimate the absolute abundance of eight immune and two stromal cell populations in each sample, including T cells, CD8 T cells, cytotoxic lymphocytes, B lineage, NK cells, monocytic lineage, myeloid dendritic cells, neutrophils, endothelial cells, and fibroblasts.

Overlap-based gene set enrichment. The enrichment of specific biological process or gene ontologies were analyzed using Enrichr, which is implemented in a R package enrichR (v3.0) [37]. Specifically, lists of DEGs were tested for significant overlaps with pre-curated gene sets within the Enrichr based on fisher exact test. The P values we utilized were the ones adjusted for multiple tests using the FDR method and the cutoff of enriched gene set term is adjusted P value < 0.05.

Survival analysis. The Kaplan-Meier curves were used to visualize differences in survival between patient groups. Cox proportional hazard (Cox PH) regression was used to assess the effect of single or multiple variables on hazard ratio. These analyses were performed using the R packages survival (v3.2.13) and visualized using survminer (v0.4.9), and survivalAnalysis (v0.3.0).

Single cell analysis. The single cell data was processed using the R package Seurat (v4.0.2). The raw count data were provided by the authors. We first normalized the raw counts using the NormalizeData() function with normalization.method="LogNormalize" and scale.factor=10000. 17 clusters were identified at resolution=0.5. Cell types of the clusters were manually annotated based on each cluster's gene markers, which were computed using FindAllMarkers() (min.pct=0.25 and logfc.threshold=0.585). The R package AUCell (v1.12.0) was used to identify gene set enrichments in the single cell transcriptome. The R package CellChat (v1.1.3) was used to visualize cell-cell communication network, grouped by different signaling pathways, among different cell types.

Statistical information. All the statistical analysis were performed using R programming language version 4.0.5. Unless otherwise stated, all the statistical tests were two tailed. In all boxplots, including gene expression, GSVA score, and gene expression ratio, P values were calculated using a two-sided Wilcoxon rank sum test. In all boxplots, the median is indicated by the line within the box and the 25th and 75th percentiles indicated by the lower and upper bounds of the box. The upper and lower lines above and below the boxes represent the whiskers. Pearson's R correlation coefficient was computed using R's *cor.test* function. The P values of the Pearson R were computed using two-sided t-test as described in the documentation. In the Kaplan-Meier survival curves, the P value is the log-rank test P value. In the Cox PH analysis, the P value shown for each variable in the graph is the result of Wald test.

Data availability

The bulk RNA-seq data were downloaded from the following online repositories. 2017_Cell_NR (ICI) was from PRJNA356761; 2020_NC_GA (ICI) was from PRJNA578193; 2015_Cell_WH (MAPKi) was from PRJNA273359, PRJNA303170, PRJNA403850; 2015_JCI_LK (MAPKi) was from EGAD00001001306. The single cell RNA-seq data were download from the GSE120575. Instead of the TPM normalized expression values, we started from the raw counts provided by the authors in personal communications. The raw count expression values were included in the source code of this study. The detailed summary of patient, sample, and cell numbers for each biopsy timing and response category is shown in **Error! Reference source not found.**A, B. All the source codes used in this study were uploaded to the GitHub repository.

References

1. Luke JJ, Schwartz GK. Chemotherapy in the management of advanced cutaneous malignant melanoma. *Clinics in Dermatology* **31**, 290-297 (2013).

2. Luke JJ, Flaherty KT, Ribas A, Long GV. Targeted agents and immunotherapies: optimizing outcomes in melanoma. *Nature Reviews Clinical Oncology* **14**, 463-482 (2017).

3. Curti BD, Faries MB. Recent Advances in the Treatment of Melanoma. *New England Journal of Medicine* **384**, 2229-2240 (2021).

4. Tawbi HA*, et al.* Relatlimab and Nivolumab versus Nivolumab in Untreated Advanced Melanoma. *New England Journal of Medicine* **386**, 24-34 (2022).

5. Alexandrov LB*, et al.* Signatures of mutational processes in human cancer. *Nature* **500**, 415-421 (2013).

6. Bruni D, Angell HK, Galon J. The immune contexture and Immunoscore in cancer prognosis and therapeutic efficacy. *Nature Reviews Cancer* **20**, 662-680 (2020).

7. Marcus L*, et al.* FDA Approval Summary: Pembrolizumab for the Treatment of Tumor Mutational Burden–High Solid Tumors. *Clinical Cancer Research* **27**, 4685-4689 (2021).

8. Hodi FS*, et al.* Improved Survival with Ipilimumab in Patients with Metastatic Melanoma. *New England Journal of Medicine* **363**, 711-723 (2010).

9. Robert C*, et al.* Pembrolizumab versus Ipilimumab in Advanced Melanoma. *New England Journal of Medicine* **372**, 2521-2532 (2015).

10. Robert C*, et al.* Nivolumab in Previously Untreated Melanoma without BRAF Mutation. *New England Journal of Medicine* **372**, 320-330 (2014).

11. Larkin J*, et al.* Combined Nivolumab and Ipilimumab or Monotherapy in Untreated Melanoma. *New England Journal of Medicine* **373**, 23-34 (2015).

12. Kalbasi A, Ribas A. Tumour-intrinsic resistance to immune checkpoint blockade. *Nature Reviews Immunology* **20**, 25-39 (2020).

13. Schoenfeld AJ, Hellmann MD. Acquired Resistance to Immune Checkpoint Inhibitors. *Cancer Cell* **37**, 443-455 (2020).

14. Nowicki TS, Hu-Lieskovan S, Ribas A. Mechanisms of Resistance to PD-1 and PD-L1 Blockade. *The Cancer Journal* **24**, 47-53 (2018).

15. Tumeh PC*, et al.* PD-1 blockade induces responses by inhibiting adaptive immune resistance. *Nature* **515**, 568-571 (2014).

16. Ayers M*, et al.* IFN-γ–related mRNA profile predicts clinical response to PD-1 blockade. *The Journal of Clinical Investigation* **127**, 2930-2940 (2017).

17. Chen P-L*, et al.* Analysis of Immune Signatures in Longitudinal Tumor Samples Yields Insight into Biomarkers of Response and Mechanisms of Resistance to Immune Checkpoint Blockade. *Cancer Discovery* **6**, 827-837 (2016).

18. Abril-Rodriguez G*, et al.* PAK4 inhibition improves PD-1 blockade immunotherapy. *Nature Cancer* **1**, 46-58 (2020).

19. Grasso CS, *et al.* Conserved Interferon-γ Signaling Drives Clinical Response to Immune Checkpoint Blockade Therapy in Melanoma. *Cancer Cell* **38**, 500-515.e503 (2020).

20. Davies H, *et al.* Mutations of the BRAF gene in human cancer. *Nature* **417**, 949-954 (2002).

21. Long GV, *et al.* Combined BRAF and MEK Inhibition versus BRAF Inhibition Alone in Melanoma. *New England Journal of Medicine* **371**, 1877-1888 (2014).

22. Larkin J, *et al.* Combined Vemurafenib and Cobimetinib in BRAF-Mutated Melanoma. *New England Journal of Medicine* **371**, 1867-1876 (2014).

23. Dummer R, *et al.* Encorafenib plus binimetinib versus vemurafenib or encorafenib in patients with BRAF-mutant melanoma (COLUMBUS): a multicentre, open-label, randomised phase 3 trial. *The Lancet Oncology* **19**, 603-615 (2018).

24. Knight DA, *et al.* Host immunity contributes to the anti-melanoma activity of BRAF inhibitors. *The Journal of Clinical Investigation* **123**, 1371-1381 (2013).

25. Song C, *et al.* Recurrent Tumor Cell–Intrinsic and –Extrinsic Alterations during MAPKi-Induced Melanoma Regression and Early Adaptation. *Cancer Discovery* **7**, 1248-1265 (2017).

26. Robert C, *et al.* Five-Year Outcomes with Dabrafenib plus Trametinib in Metastatic Melanoma. *New England Journal of Medicine* **381**, 626-636 (2019).

27. Ascierto PA, *et al.* 5-Year Outcomes with Cobimetinib plus Vemurafenib in BRAFV600 Mutation–Positive Advanced Melanoma: Extended Follow-up of the coBRIM Study. *Clinical Cancer Research* **27**, 5225-5235 (2021).

28. Atkins MB, *et al.* Comparative efficacy of combination immunotherapy and targeted therapy in the treatment of BRAF-mutant advanced melanoma: a matching-adjusted indirect comparison. *Immunotherapy* **11**, 617-629 (2019).

29. Riaz N, *et al.* Tumor and Microenvironment Evolution during Immunotherapy with Nivolumab. *Cell* **171**, 934-949.e916 (2017).

30. Hugo W, *et al.* Non-genomic and Immune Evolution of Melanoma Acquiring MAPKi Resistance. *Cell* **162**, 1271-1285 (2015).

31. Kwong LN, *et al.* Co-clinical assessment identifies patterns of BRAF inhibitor resistance in melanoma. *The Journal of Clinical Investigation* **125**, 1459-1470 (2015).

32. Lowery FJ, *et al.* Molecular signatures of antitumor neoantigen-reactive T cells from metastatic human cancers. *Science* **375**, 877-884 (2022).

33. Helmink BA, *et al.* B cells and tertiary lymphoid structures promote immunotherapy response. *Nature* **577**, 549-555 (2020).

34. Cabrita R, *et al.* Tertiary lymphoid structures improve immunotherapy and survival in melanoma. *Nature* **577**, 561-565 (2020).

35. Petitprez F, *et al.* B cells are associated with survival and immunotherapy response in sarcoma. *Nature* **577**, 556-560 (2020).

36. Meylan M, *et al.* Tertiary lymphoid structures generate and propagate anti-tumor antibody-producing plasma cells in renal cell cancer. *Immunity* **55**, 527-541.e525 (2022).

37. Kuleshov MV, *et al.* Enrichr: a comprehensive gene set enrichment analysis web server 2016 update. *Nucleic Acids Research* **44**, W90-W97 (2016).

38. Sade-Feldman M, *et al.* Defining T Cell States Associated with Response to Checkpoint Immunotherapy in Melanoma. *Cell* **175**, 998-1013.e1020 (2018).

39. Long GV, *et al.* Increased MAPK reactivation in early resistance to dabrafenib/trametinib combination therapy of BRAF-mutant metastatic melanoma. *Nat Commun* **5**, 5694 (2014).

40. Rizos H, *et al.* BRAF inhibitor resistance mechanisms in metastatic melanoma: spectrum and clinical impact. *Clin Cancer Res* **20**, 1965-1977 (2014).

41. Forster R, Davalos-Misslitz AC, Rot A. CCR7 and its ligands: balancing immunity and tolerance. *Nat Rev Immunol* **8**, 362-371 (2008).

42. De Silva NS, Klein U. Dynamics of B cells in germinal centres. *Nature Reviews Immunology* **15**, 137-148 (2015).

43. Beltra J-C, *et al.* Developmental Relationships of Four Exhausted CD8+ T Cell Subsets Reveals Underlying Transcriptional and Epigenetic Landscape Control Mechanisms. *Immunity* **52**, 825-841.e828 (2020).

44. Jenh CH, *et al.* Human B cell-attracting chemokine 1 (BCA-1; CXCL13) is an agonist for the human CXCR3 receptor. *Cytokine* **15**, 113-121 (2001).

45. Aibar S, *et al.* SCENIC: single-cell regulatory network inference and clustering. *Nature Methods* **14**, 1083-1086 (2017).

46. Cyster JG, Allen CDC. B Cell Responses: Cell Interaction Dynamics and Decisions. *Cell* **177**, 524-540 (2019).

47. Ise W, *et al.* T Follicular Helper Cell-Germinal Center B Cell Interaction Strength Regulates Entry into Plasma Cell or Recycling Germinal Center Cell Fate. *Immunity* **48**, 702-715 e704 (2018).

48. Zhou JHS, Markham JF, Duffy KR, Hodgkin PD. Stochastically Timed Competition Between Division and Differentiation Fates Regulates the Transition From B Lymphoblast to Plasma Cell. *Front Immunol* **9**, 2053 (2018).

49. Kretschmer B, Kuhl S, Fleischer B, Breloer M. Activated T cells induce rapid CD83 expression on B cells by engagement of CD40. *Immunol Lett* **136**, 221-227 (2011).

50. Lee-Chang C, *et al.* Activation of 4-1BBL+ B cells with CD40 agonism and IFNγ elicits potent immunity against glioblastoma. *Journal of Experimental Medicine* **218**, (2020).

51. Cui C, *et al.* Neoantigen-driven B cell and CD4 T follicular helper cell collaboration promotes anti-tumor CD8 T cell responses. *Cell* **184**, 6101-6118.e6113 (2021).

52. Song L, Cohen D, Ouyang Z, Cao Y, Hu X, Liu XS. TRUST4: immune repertoire reconstruction from bulk and single-cell RNA-seq data. *Nature Methods* **18**, 627-630 (2021).

53. Nouri N, Kleinstein SH. Somatic hypermutation analysis for improved identification of B cell clonal families from next-generation sequencing data. *PLOS Computational Biology* **16**, e1007977 (2020).

54. Somasundaram R, *et al.* Tumor-associated B-cells induce tumor heterogeneity and therapy resistance. *Nature Communications* **8**, 607 (2017).

55. Yost KE, *et al.* Clonal replacement of tumor-specific T cells following PD-1 blockade. *Nature Medicine* **25**, 1251-

1259 (2019).

56. Li H, *et al.* Dysfunctional CD8 T Cells Form a Proliferative, Dynamically Regulated Compartment within Human Melanoma. *Cell* **176**, 775-789.e718 (2019).

57. Workel HH, *et al.* A Transcriptionally Distinct CXCL13(+)CD103(+)CD8(+) T-cell Population Is Associated with B-cell Recruitment and Neoantigen Load in Human Cancer. *Cancer Immunol Res* **7**, 784-796 (2019).

58. Crotty S. T Follicular Helper Cell Biology: A Decade of Discovery and Diseases. *Immunity* **50**, 1132-1148 (2019).

59. Victora GD, Nussenzweig MC. Germinal centers. *Annu Rev Immunol* **30**, 429-457 (2012).

60. Prazma CM, Yazawa N, Fujimoto Y, Fujimoto M, Tedder TF. CD83 expression is a sensitive marker of activation required for B cell and CD4+ T cell longevity in vivo. *J Immunol* **179**, 4550-4562 (2007).

61. Wennhold K, *et al.* CD40-activated B cells induce anti-tumor immunity in vivo. *Oncotarget* **8**, 27740-27753 (2017).

62. Sagiv-Barfi I, Czerwinski DK, Shree T, Lohmeyer JJK, Levy R. Intratumoral immunotherapy relies on B and T cell collaboration. *Sci Immunol* **7**, eabn5859 (2022).

63. Jiang Q, *et al.* CD19(+) tumor-infiltrating B-cells prime CD4(+) T-cell immunity and predict platinum-based chemotherapy efficacy in muscle-invasive bladder cancer. *Cancer Immunol Immunother* **68**, 45-56 (2019).

64. Mounzer RH, *et al.* Lymphotoxin-alpha contributes to lymphangiogenesis. *Blood* **116**, 2173-2182 (2010).

65. Zhang Q, *et al.* Increased lymphangiogenesis in joints of mice with inflammatory arthritis. *Arthritis Research & Therapy* **9**, R118 (2007).

66. Rehal S, von der Weid P-Y. TNFΔARE Mice Display Abnormal Lymphatics and Develop Tertiary Lymphoid Organs in the Mesentery. *The American Journal of Pathology* **187**, 798-807 (2017).

67. Luther SA, *et al.* Differing Activities of Homeostatic Chemokines CCL19, CCL21, and CXCL12 in Lymphocyte and Dendritic Cell Recruitment and Lymphoid Neogenesis. *The Journal of Immunology* **169**, 424-433 (2002).

68. Luther SA, Lopez T, Bai W, Hanahan D, Cyster JG. BLC Expression in Pancreatic Islets Causes B Cell Recruitment and Lymphotoxin-Dependent Lymphoid Neogenesis. *Immunity* **12**, 471-481 (2000).

69. Ukita M, *et al.* CXCL13-producing CD4+ T cells accumulate in the early phase of tertiary lymphoid structures in ovarian cancer. *JCI Insight* **7**, (2022).

70. van Hooren L, *et al.* Agonistic CD40 therapy induces tertiary lymphoid structures but impairs responses to checkpoint blockade in glioma. *Nat Commun* **12**, 4127 (2021).

71. Perez CR, De Palma M. Engineering dendritic cell vaccines to improve cancer immunotherapy. *Nat Commun* **10**, 5408 (2019).

72. Subramanian A, *et al.* Gene set enrichment analysis: A knowledge-based approach for interpreting genome-wide expression profiles. *Proceedings of the National Academy of Sciences* **102**, 15545-15550 (2005).

73. Liberzon A, Birger C, Thorvaldsdóttir H, Ghandi M, Mesirov Jill P, Tamayo P. The Molecular Signatures Database Hallmark Gene Set Collection. *Cell Systems* **1**, 417-425 (2015).

74. Hänzelmann S, Castelo R, Guinney J. GSVA: gene set variation analysis for microarray and RNA-Seq data. *BMC Bioinformatics* **14**, 7 (2013).

75. Vander Heiden JA*, et al.* AIRR Community Standardized Representations for Annotated Immune Repertoires. *Frontiers in Immunology* **9**, (2018).

76. Nguyen TV, Pawlikowska P, Firlej V, Rosselli F, Aoufouchi S. V(D)J recombination process and the Pre-B to immature B-cells transition are altered in Fanca−/− mice. *Scientific Reports* **6**, 36906 (2016).

77. Gupta NT, Vander Heiden JA, Uduman M, Gadala-Maria D, Yaari G, Kleinstein SH. Change-O: a toolkit for analyzing large-scale B cell immunoglobulin repertoire sequencing data. *Bioinformatics* **31**, 3356-3358 (2015).

Acknowledgments

This study was funded in part by the NIH/NCI grant (1R01CA236910) and grant from Parker Institute for Cancer Immunotherapy. L.D is supported by grant from Parker Institute for Cancer Immunotherapy at UCLA. W.H is supported the NIH/NCI grant (1R01CA236910), the Melanoma Research Alliance, the Margaret E. Early Medical Research Trust Grant, and the Parker Institute for Cancer Immunotherapy at UCLA. We thank Moshe Sade-Feldman and Nir Hacohen for generously providing the raw count expression data of single cell RNA-seq used in their publication.

Author contributions

L.D, W.H. designed the experiments and analyses. L.D. performed the analyses unless specified. L.S. developed the single cell analysis pipeline. All authors reviewed and approved the manuscript.

Competing interests

The authors declare no competing interests.

Materials and Correspondence

Correspondence and requests for materials should be addressed to hwilly@mednet.ucla.edu

Additional information

Supplementary information is available for this paper online

Figure Legends

Main figures

Fig 1: Response to ICI and MAPKi therapy are both associated with increased T cell infiltration and enhanced IFNγ pathway activity in the tumor.

A) Schematic of comparative analysis between transcriptomic response to ICI and MAPKi therapy.

B) The number of differentially upregulated genes in ICI OT-R (red), MAPKi OT-R (black) or both (blue). The differentially expressed genes (DEGs) are computed with respect to the OT-NR samples of each group.

C) Enriched cell marker genes (based on Human Gene Atlas using Enrichr tool) in ICI-specific, MAPKi-specific, and ICI and MAPKi-shared DEGs in (B).

D) Normalized expression of T cell marker genes *CD3D* and *CD8B* in the PT, OT-R and OT-NR samples of patients under ICI and MAPKi therapy. The dataset cohort of the datapoints is listed in the righmost legend.

E) Normalized expression of T cell activation genes *IFNG*, *GZMB* and *PRF1* in the PT, OT-R and OT-NR samples of patients under ICI and MAPKi therapy.

F) GSVA gene set enrichment scores of the hallmark interferon gamma gene set. Both therapies induced a similar increase in interferon gamma pathway downstream genes.

G) Change in the expression ratio between the listed T cell cytolytic genes and *CD8B* in patient-matched PT and OT-R tumors or PT and OT-NR tumors.

H) Kaplan-Meier survival curves of ICI- or MAPKi-treated melanoma patients stratified by either *CD8B* expression (left) or hallmark interferon gamma response gene set scores (right) in their OT tumors.

Fig 2: Relative increase of B cell and tertiary lymphoid structure (TLS) marker genes in response to ICI therapy compared to MAPKi.

A) Enriched tissue specific gene sets in DEGs upregulated in ICI OT-R tumors with respect to MAPKi OT-

R tumors (after adjustment by respective therapy group's OT-NR tumors; see Methods).
B) Normalized expression of B cell marker genes and enrichment of B cell lineage gene set among the PT, OT-R and OT-NR tumors in the ICI or MAPKi therapy group.
C, D) Normalized expression of TLS-related genes, *CXCR5*, *BCL6*, *CXCL13* and *CCL21* among the PT, OT-R and OT-NR tumors in the ICI or MAPKi therapy group.
E) Kaplan-Meier survival curves of ICI- or MAPKi-treated melanoma patients stratified by either *CD19* expression (left) or TLS gene set enrichment score (right) in their OT tumors.

Fig 3: Increased B cell proportion is associated with TLS marker enrichments and improved OS in an independent cohort of ICI treated melanoma.
A) UMAP projection of intratumoral CD45+ cells of ICI-treated melanoma. The cell type annotation of each cell cluster was inferred from the DEGs of each cluster.
B, C) Normalized expression of markers of cell type/activity among different T and NK cell (B) or B cell and myeloid cell populations (C).
D) The fraction of the T, NK B and plasma cell populations in stratified by response vs. resistance to ICI in PT (top) and OT tumors (bottom). The boxplots are colored to match the cell clusters in (A).
E) Kaplan-Meier survival curves of ICI-treated patients stratified by the proportion of B cells within either their PT (top) or OT tumors (bottom).
F, G) Normalized expression of germinal center (GC) B cell markers, *BCL6* and *REL,* or follicular helper T cells (Tfh), *CXCR5* and *CXCL13*, within the listed T/B cell populations from the scRNA-seq.
H) Predicted enrichment of receptor-ligand interaction involving the CXCL chemokine signaling in the ICI OT samples (left; the color of the connecting edge is the source cell's) and the normalized expression of the chemokine and their receptors in each immune population (right). The interaction involving the CXCL13-CXCR5 pair between tumor reactive, *PDCD1*+ *TOX*+ CD8 T cells and B cells was significant in ICI OT-R tumors.

Fig 4: B cells in ICI OT-R tumors present antigens to *PDCD1*+ *TOX*+ tumor-reactive CD8 T and CD4 Tfh cells via the MHC I and II pathways.
A) Predicted enrichment of cell-to-cell interaction through MHC II antigen presentation pathway (left) and the normalized expression of MHC II-related genes (right). The expressions of MHC II genes are similar between ICI OT-R and OT-NR but, because of the higher proportion of B cells in ICI OT-R, the predicted MHC II interaction is (relatively) dominated by B cells in ICI OT-R. The interaction is more evenly distributed among the monocytic DC, macrophages, and B cells in ICI OT-NR tumors.
B) Normalized expression of *CD40LG* and *CD83* in follicular helper T cell (Tfh) and GC B cell populations, respectively.
C) Predicted enrichment of cell-to-cell interaction through CD40L/CD40 pathway specific to ICI OT-R tumors (left) and the normalized expression of CD40 pathway related genes (right).
D) BCR clonotype diversity and clonality among the PT, OT-R and OT-NR tumors in the ICI or MAPKi therapy group. The BCR clones are based on TRUST4's predicted CDR3 sequences of the immunoglobulin heavy (IGH) chains in each RNA-seq sample (see Methods).
E) Somatic hypermutation (SHM) frequencies based on predicted germline (i.e. prior to SHM) BCR clones by SCOPer (see Methods). The fraction is calculated as the number of germline BCR clones with more than one SHM-generated, mature BCR clones.
F) Kaplan-Meier survival curves of ICI- or MAPKi-treated melanoma patients in the bulk RNA-seq datasets stratified by either the BCR diversity (left) or clonality (right) of their OT tumors.
G) Kaplan-Meier survival curves of ICI-treated patients in the scRNA-seq dataset stratified either the BCR diversity (left) or clonality (right) of their OT tumors.

Fig 5: BCR diversity and IFNγ pathway activation are significant factors associated with enhanced OS after ICI therapy.

A) Predicted enrichment of receptor-ligand interaction involving type II IFN signaling between *IFNG* expression CD8 T cell clusters and B cells in ICI OT-R tumors (top). Increased expression of *IFNGR1/R2* in the B cells of ICI-responders (bottom) is expected to further enhance B cells' antigen presentation activity.

B) Kaplan-Meier survival curves of patients stratified by BCR diversity and hallmark interferon gamma gene set score in OT tumors of the ICI or MAPKi therapy group.

C) Multivariate Cox proportional hazards analysis assessing the hazard ratios of BCR diversity and hallmark interferon gamma gene set score in ICI OT tumor samples.

D) The schematic of our proposed model of productive ICI response. First, tumor-reactive CD8 T cells produced CXCL13 in response to ICI to recruit TLS-associated CXCR5+ Tfh and B cells. B cells pick up tumor antigens from the debris of tumor cells killed by the CD8 T cells. Successful tumor antigen presentation by B cells, expected to highly correlate with their BCR repertoire diversity, results in the activation of Tfh and tumor-reactive CD8 T cells. Tfh and CD8 T cells upregulates of *CD40LG* and *IFNG*, respectively, resulting in enhancement of B cell antigen presentation activity. Finally, activated, tumor reactive CD8 T cells kill more tumor cells and secrete more CXCL13 to recruit additional CXCR5+ Tfh and B cells, thus forming a positive cycle of antitumor immune response.

Supplementary figures

Supp. Fig 1: Shared and therapy-specific transcriptomic changes after ICI and MAPKi therapy.

A) Schematic of the bulk RNA-seq data sets of ICI- and MAPKi-treated melanoma used in this study.

B) T cell enrichment scores computed by MCPcounter in the PT, OT-R and OT-NR samples of patients under ICI and MAPKi therapy.

C) Normalized expression of T cell marker genes *CD3D* and *CD8B* in the PT, OT-R and OT-NR samples of patients under ICI and MAPKi therapy (inter therapy comparison).

D) Change in the expression ratio of *IFNG* to *CD8B* in patient-matched PT and OT-R tumors or PT and OT-NR tumors.

E) Correlation between PFS and OS after MAPKi therapy across two separate melanoma datasets.

F) Kaplan-Meier survival curves of ICI- or MAPKi-treated melanoma patients stratified by either *CD8B* expression (left) or hallmark interferon gamma response gene set scores (right) in their PT tumors.

Supp. Fig 2: Characterization of B cell and TLS-related gene expression changes after ICI and MAPKi therapy.

A) Enriched tissue specific gene sets in DEGs upregulated in MAPKi OT-R tumors with respect to ICI OT-R tumors (after adjustment by respective therapy group's OT-NR tumors).

B) Normalized expression of the listed B cell-related genes among the PT, OT-R and OT-NR tumors in the ICI or MAPKi therapy group.

C) (top) Pairwise expression comparison of the listed B cell-related genes between the PT samples of melanoma patients who will subsequently respond (R) or not respond (NR) to ICI. (bottom) The same comparison applied on the OT tumors ICI treated patients.

D) Enrichment scores of a recently published TLS 7-gene and 9-gene gene sets among the PT, OT-R and OT-NR tumors in the ICI or MAPKi therapy group.

E) Kaplan-Meier survival curves of ICI- or MAPKi-treated melanoma patients stratified by either *CD19* expression (left) or TLS gene set enrichment score (right) in their PT tumors.

Supp. Fig 3: Single cell analysis of ICI-treated melanoma.

A) The fraction of the myeloid and proliferating cell populations in stratified by response vs. resistance to ICI in PT (top) and OT tumors (bottom).
B) Kaplan-Meier survival curves of ICI-treated patients stratified by the proportion of monocyte/monocyte-derived macrophages within either their PT (top) or OT tumors (bottom).
C) Single cell-based gene set enrichment score of the TLS 7-gene and 9-gene signatures projected on the UMAP (left) or presented in boxplot across all cell types (right). The scores were separated into quartiles to assist the visualization of high and low gene set enrichments in different cell populations.

Supp. Fig 4: B cell-associated antigen presentation and clonotype analyses.
A) CellChat inferred cell-cell communication among the intratumoral immune populations across different curated signaling pathways. The interactions are grouped based on ICI response vs. no-response in either PT or OT tumors.
B) Predicted enrichment of cell-to-cell interaction through MHC II antigen presentation pathway.
C, D) Change in BCR (C) or TCR (D) clonal fraction in grouped by clones found only in the OT sample (OT-specific), only in the PT (PT-specific) and both in the PT and OT samples (overlapping, see illustration on the left). These fractions are calculated with respect to the union of all BCR/TCR clones found in the PT and OT samples of each patient; this analysis is done only on patients with PT and OT tumors.

Supp. Fig 5: Multivariate analysis of survival examining the association of T cell and B cell related variables to patient OS after ICI therapy.
A) Kaplan-Meier survival curves of patients stratified by normalized expressions of *CD8B* and *CD19* in either PT or OT tumors of the ICI or MAPKi therapy group.
B) Multivariate Cox proportional hazards analysis assessing the hazard ratios of BCR diversity, hallmark interferon gamma gene set score, and their interaction in ICI OT tumor samples.

Supplementary data

Supp. Table 1 : Clinical characteristics, gene expression and gene set enrichments in the bulk RNA-seq datasets.
A) Summary of clinical data associated with the tumor samples (bulk and scRNA-seq datasets).
B) Normalized expression matrix (log2 cpm, batch effect corrected) of the bulk RNA-seq data of ICI or MAPKi-treated tumors.
C) Difference in fold changes of OT-R vs. OT-NR samples after ICI or MAPKi therapy.
D) Gene sets/cell markers enriched in tumors responding to ICI, MAPKi or both (Enrichr analysis).
E) The relative abundance of immune and stromal cell populations in each sample in bulk RNA-seq dataset (MCPcounter analysis).
F) GSVA score matrix of selected gene sets of the bulk RNA-seq data of ICI or MAPKi-treated tumors.
G) TCR and BCR clonotype repertoire metrics of the ICI and MAPKi datasets (bulk and scRNA-seq).

Supp. Table 2: PFS and OS correlation in MAPKi-treated melanoma patients.
A) OS and PFS data from two MAPKi treated gene expression microarray datasets (Rizos et al CCR 2014 and Long et al Nat. Comm. 2014).

Supp. Table 3: Cell type fraction, DEGs and survival analysis of scRNA-Seq data set of ICI-treated melanoma.
A) Differentially upregulated genes in each single cell cluster of CD45+ cells from ICI-treated tumors.
B) The fraction of immune cell populations in each PT/OT tumor sample of ICI-treated melanoma patients.
C) The association between the fraction each immune population (in PT or OT tumors) and OS after ICI therapy.

D) Differentially expressed genes in PT and OT tumors based on response (R) vs. no-response (NR) to ICI.
E) The association between TCR/BCR clonality or diversity in PT or OT tumors and OS after ICI therapy.

Supp. Table 4: Univariate and multivariate survival analyses of B cell, T cell and TLS-related gene/gene sets.
A) Univariate CoxPH analysis of survival of B cell, T cell and TLS-related gene/gene sets (bulk RNA-seq cohorts).
B) Multivariate CoxPH analysis of survival of significant B cell, T cell and TLS-related gene/gene sets (ICI-OT only, pairwise independent).
C) Multivariate CoxPH analysis of survival of significant B cell, T cell and TLS-related gene/gene sets (ICI-OT only, with pairwise interaction term).

Figure 1

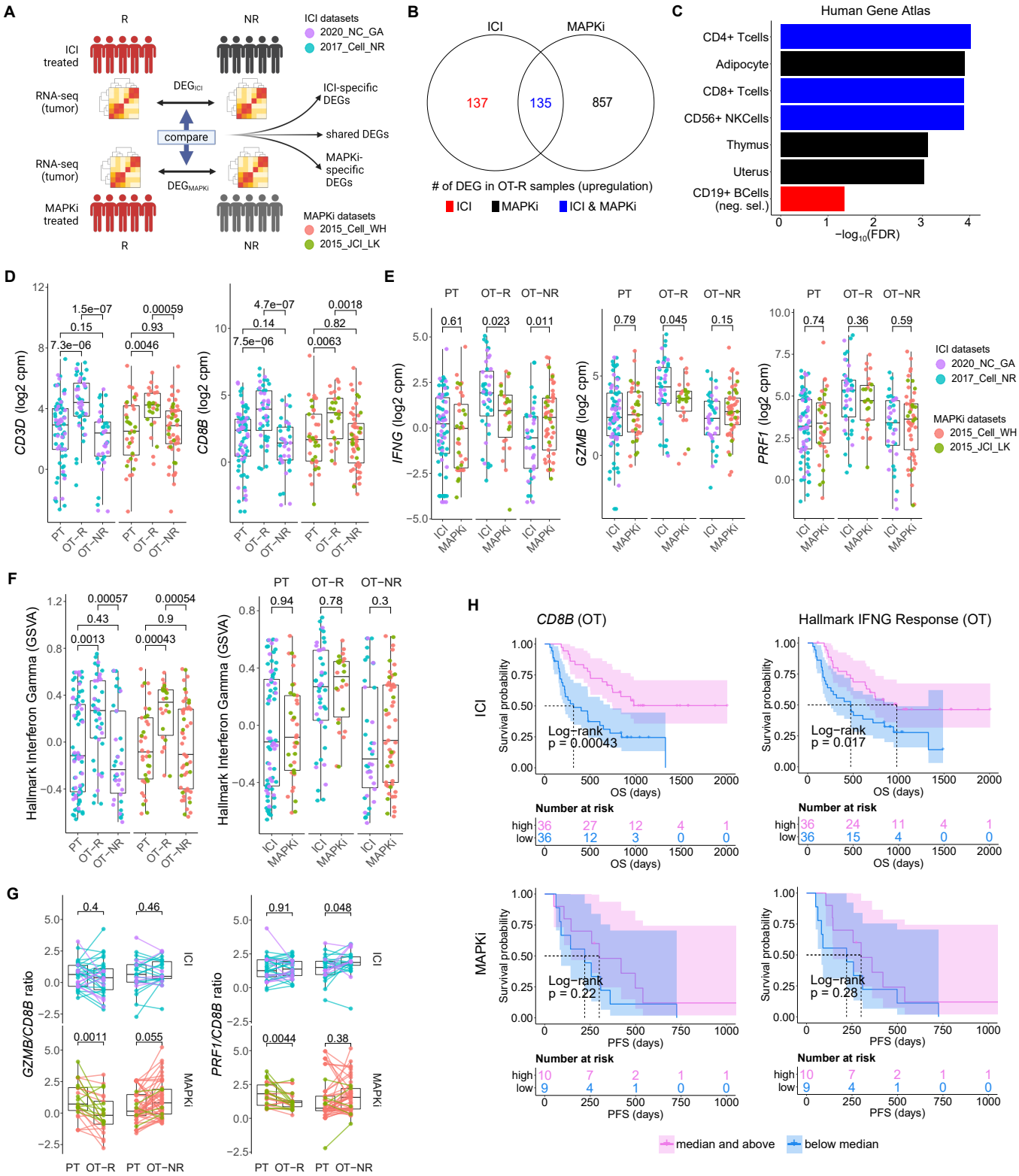
A
R
NR
ICI treated
RNA-seq (tumor)
DEG_ICI
compare
RNA-seq (tumor)
DEG_MAPKi
MAPKi treated
R
NR
ICI datasets
2020_NC_GA
2017_Cell_NR
ICI-specific DEGs
shared DEGs
MAPKi-specific DEGs
MAPKi datasets
2015_Cell_WH
2015_JCI_LK
B
ICI
MAPKi
137
135
857
# of DEG in OT-R samples (upregulation)
ICI
MAPKi
ICI & MAPKi
C
Human Gene Atlas
CD4+ Tcells
Adipocyte
CD8+ Tcells
CD56+ NKCells
Thymus
Uterus
CD19+ BCells (neg. sel.)
−log10(FDR)
D
CD3D (log2 cpm)
CD8B (log2 cpm)
PT
OT−R
OT−NR
E
IFNG (log2 cpm)
GZMB (log2 cpm)
PRF1 (log2 cpm)
ICI
MAPKi
F
Hallmark Interferon Gamma (GSVA)
G
GZMB/CD8B ratio
PRF1/CD8B ratio
H
CD8B (OT)
Hallmark IFNG Response (OT)
Survival probability
Log−rank p = 0.00043
Log−rank p = 0.017
Log−rank p = 0.22
Log−rank p = 0.28
OS (days)
PFS (days)
Number at risk
high
low
median and above
below median

Figure 2

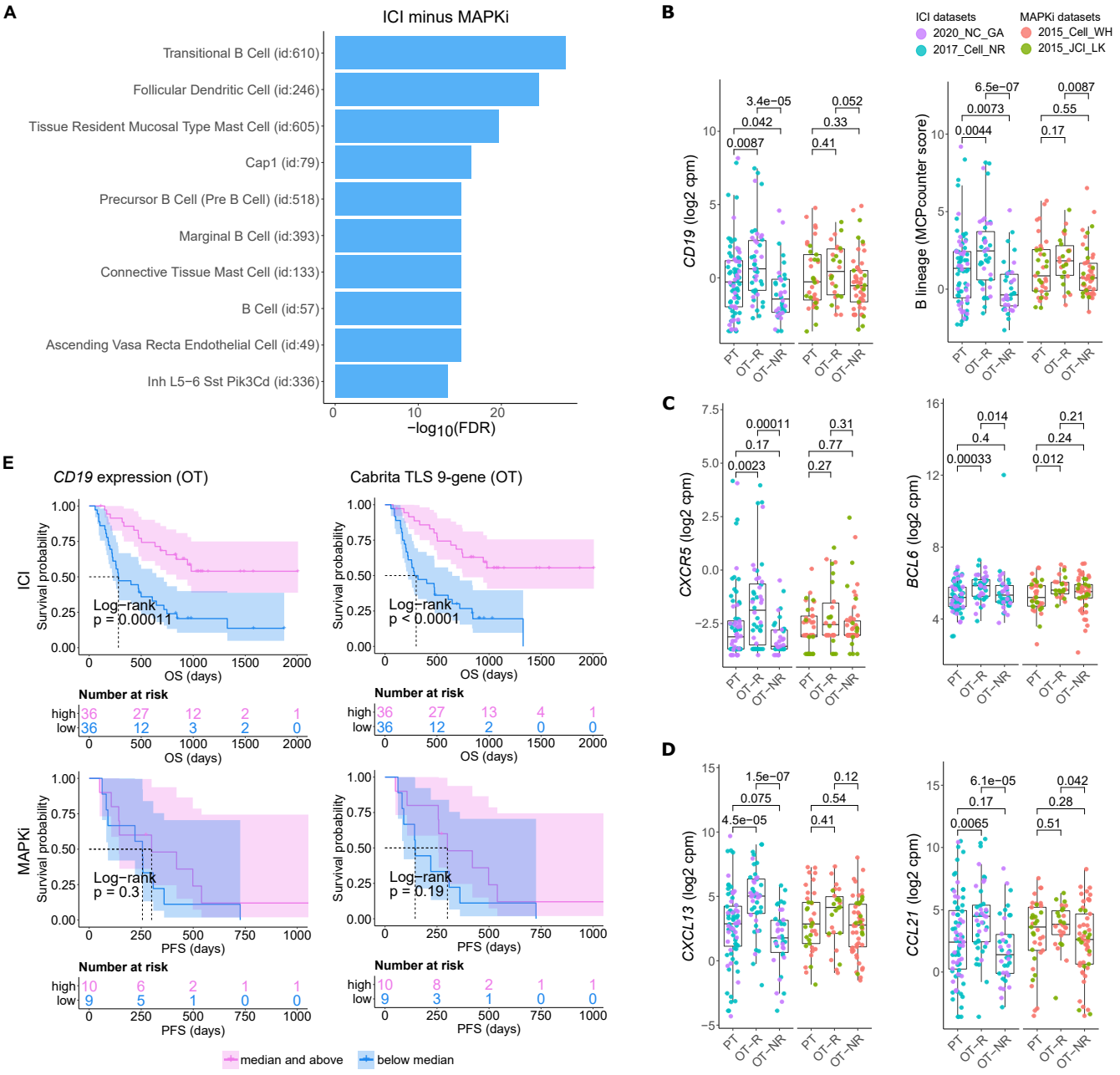
A
ICI minus MAPKi
Transitional B Cell (id:610)
Follicular Dendritic Cell (id:246)
Tissue Resident Mucosal Type Mast Cell (id:605)
Cap1 (id:79)
Precursor B Cell (Pre B Cell) (id:518)
Marginal B Cell (id:393)
Connective Tissue Mast Cell (id:133)
B Cell (id:57)
Ascending Vasa Recta Endothelial Cell (id:49)
Inh L5−6 Sst Pik3Cd (id:336)
−log10(FDR)
B
ICI datasets
2020_NC_GA
2017_Cell_NR
MAPKi datasets
2015_Cell_WH
2015_JCI_LK
CD19 (log2 cpm)
B lineage (MCPcounter score)
PT
OT−R
OT−NR
C
CXCR5 (log2 cpm)
BCL6 (log2 cpm)
D
CXCL13 (log2 cpm)
CCL21 (log2 cpm)
E
CD19 expression (OT)
Cabrita TLS 9-gene (OT)
ICI
MAPKi
Survival probability
Log−rank p = 0.00011
Log−rank p < 0.0001
Log−rank p = 0.3
Log−rank p = 0.19
OS (days)
PFS (days)
Number at risk
high
low
median and above
below median

G

Figure 3

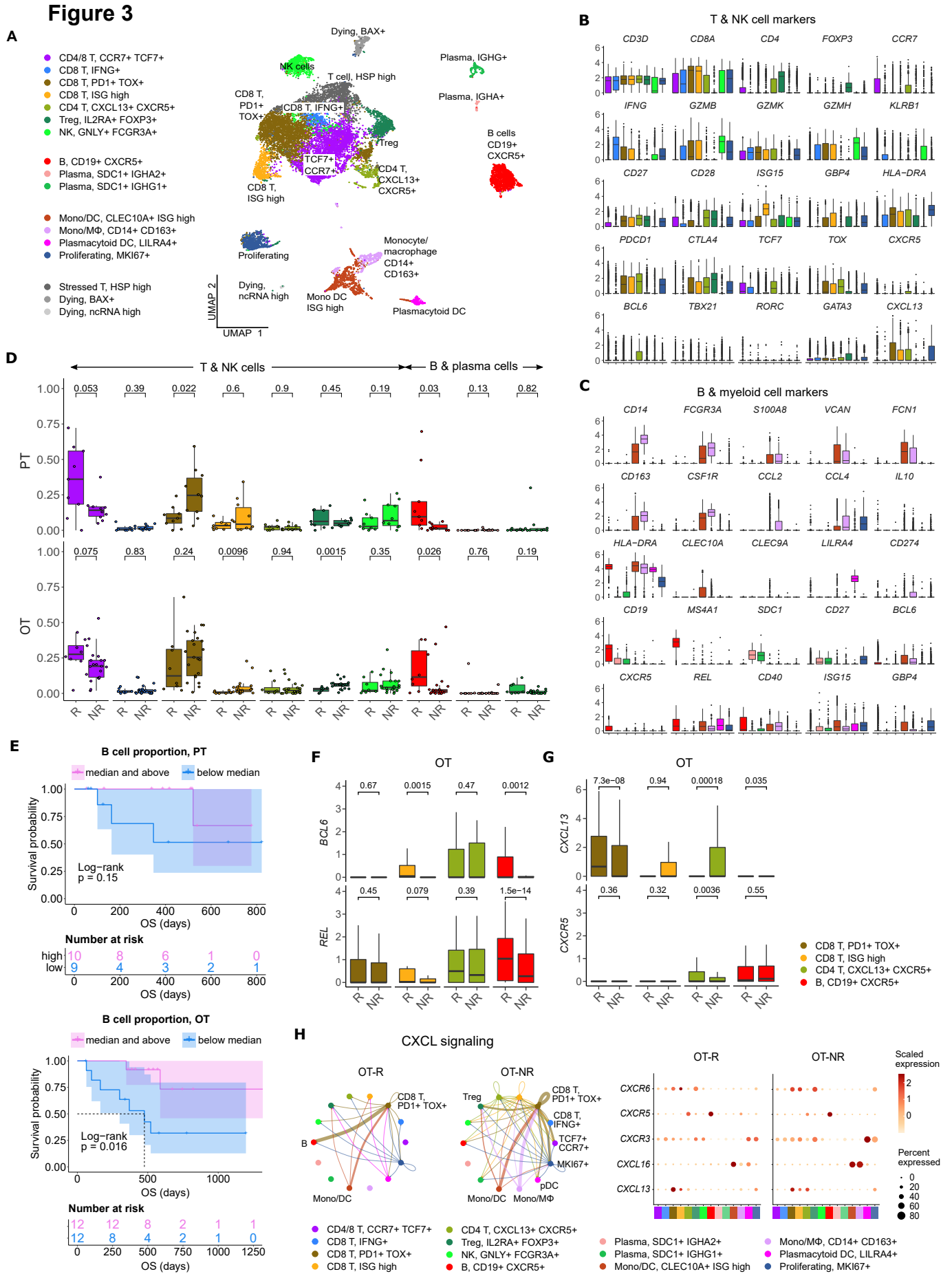
A
CD4/8 T, CCR7+ TCF7+
CD8 T, IFNG+
CD8 T, PD1+ TOX+
CD8 T, ISG high
CD4 T, CXCL13+ CXCR5+
Treg, IL2RA+ FOXP3+
NK, GNLY+ FCGR3A+
B, CD19+ CXCR5+
Plasma, SDC1+ IGHA2+
Plasma, SDC1+ IGHG1+
Mono/DC, CLEC10A+ ISG high
Mono/MΦ, CD14+ CD163+
Plasmacytoid DC, LILRA4+
Proliferating, MKI67+
Stressed T, HSP high
Dying, BAX+
Dying, ncRNA high
Dying, BAX+
NK cells
T cell, HSP high
Plasma, IGHG+
Plasma, IGHA+
CD8 T, PD1+ TOX+
CD8 T, IFNG+
Treg
B cells CD19+ CXCR5+
TCF7+ CCR7+
CD4 T, CXCL13+ CXCR5+
CD8 T, ISG high
Proliferating
Monocyte/ macrophage CD14+ CD163+
Dying, ncRNA high
Mono DC ISG high
Plasmacytoid DC
UMAP 2
UMAP 1
B
T & NK cell markers
CD3D CD8A CD4 FOXP3 CCR7
IFNG GZMB GZMK GZMH KLRB1
CD27 CD28 ISG15 GBP4 HLA−DRA
PDCD1 CTLA4 TCF7 TOX CXCR5
BCL6 TBX21 RORC GATA3 CXCL13
C
B & myeloid cell markers
CD14 FCGR3A S100A8 VCAN FCN1
CD163 CSF1R CCL2 CCL4 IL10
HLA−DRA CLEC10A CLEC9A LILRA4 CD274
CD19 MS4A1 SDC1 CD27 BCL6
CXCR5 REL CD40 ISG15 GBP4
D
T & NK cells
B & plasma cells
PT
OT
0.053 0.39 0.022 0.6 0.9 0.45 0.19 0.03 0.13 0.82
0.075 0.83 0.24 0.0096 0.94 0.0015 0.35 0.026 0.76 0.19
R NR
E
B cell proportion, PT
median and above
below median
Survival probability
Log−rank p = 0.15
OS (days)
Number at risk
high 10 8 6 1 0
low 9 4 3 2 1
B cell proportion, OT
Log−rank p = 0.016
Number at risk
12 12 8 2 1 1
12 8 4 2 1 0
F
OT
BCL6
REL
0.67 0.0015 0.47 0.0012
0.45 0.079 0.39 1.5e−14
G
OT
CXCL13
CXCR5
7.3e−08 0.94 0.00018 0.035
0.36 0.32 0.0036 0.55
CD8 T, PD1+ TOX+
CD8 T, ISG high
CD4 T, CXCL13+ CXCR5+
B, CD19+ CXCR5+
H
CXCL signaling
OT-R
OT-NR
CD8 T, PD1+ TOX+
B
Mono/DC
Treg
CD8 T, IFNG+
TCF7+ CCR7+
MKI67+
pDC
Mono/MΦ
CXCR6
CXCR5
CXCR3
CXCL16
CXCL13
Scaled expression
Percent expressed
CD4/8 T, CCR7+ TCF7+
CD8 T, IFNG+
CD8 T, PD1+ TOX+
CD8 T, ISG high
CD4 T, CXCL13+ CXCR5+
Treg, IL2RA+ FOXP3+
NK, GNLY+ FCGR3A+
B, CD19+ CXCR5+
Plasma, SDC1+ IGHA2+
Plasma, SDC1+ IGHG1+
Mono/DC, CLEC10A+ ISG high
Mono/MΦ, CD14+ CD163+
Plasmacytoid DC, LILRA4+
Proliferating, MKI67+

Figure 4

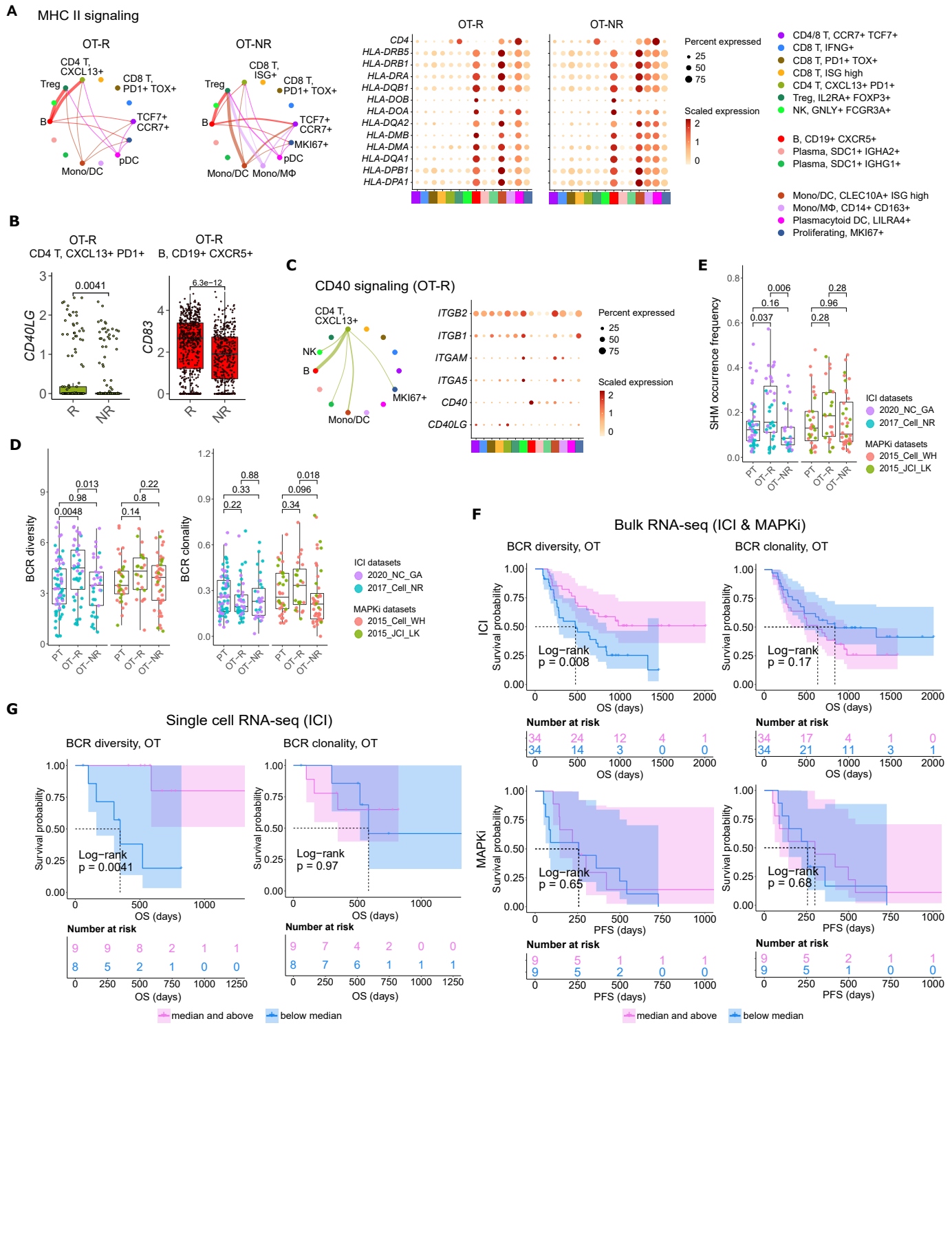
A
MHC II signaling
OT-R
OT-NR
CD4 T, CXCL13+
CD8 T, PD1+ TOX+
Treg
B
TCF7+ CCR7+
pDC
Mono/DC
CD8 T, ISG+
MKI67+
Mono/MΦ
CD4
HLA-DRB5
HLA-DRB1
HLA-DRA
HLA-DQB1
HLA-DOB
HLA-DOA
HLA-DQA2
HLA-DMB
HLA-DMA
HLA-DQA1
HLA-DPB1
HLA-DPA1
Percent expressed
25
50
75
Scaled expression
2
1
0
CD4/8 T, CCR7+ TCF7+
CD8 T, IFNG+
CD8 T, PD1+ TOX+
CD8 T, ISG high
CD4 T, CXCL13+ PD1+
Treg, IL2RA+ FOXP3+
NK, GNLY+ FCGR3A+
B, CD19+ CXCR5+
Plasma, SDC1+ IGHA2+
Plasma, SDC1+ IGHG1+
Mono/DC, CLEC10A+ ISG high
Mono/MΦ, CD14+ CD163+
Plasmacytoid DC, LILRA4+
Proliferating, MKI67+
B
OT-R
CD4 T, CXCL13+ PD1+
OT-R
B, CD19+ CXCR5+
CD40LG
CD83
0.0041
6.3e−12
R
NR
C
CD40 signaling (OT-R)
CD4 T, CXCL13+
NK
B
MKI67+
Mono/DC
ITGB2
ITGB1
ITGAM
ITGA5
CD40
CD40LG
Percent expressed
25
50
75
Scaled expression
2
1
0
E
SHM occurrence frequency
0.006
0.16
0.037
0.28
0.96
0.28
PT
OT−R
OT−NR
ICI datasets
2020_NC_GA
2017_Cell_NR
MAPKi datasets
2015_Cell_WH
2015_JCI_LK
D
BCR diversity
BCR clonality
0.013
0.98
0.0048
0.22
0.8
0.14
0.88
0.33
0.22
0.018
0.096
0.34
PT
OT−R
OT−NR
ICI datasets
2020_NC_GA
2017_Cell_NR
MAPKi datasets
2015_Cell_WH
2015_JCI_LK
F
Bulk RNA-seq (ICI & MAPKi)
BCR diversity, OT
BCR clonality, OT
ICI
Survival probability
Log−rank
p = 0.008
Log−rank
p = 0.17
OS (days)
Number at risk
34 24 12 4 1
34 14 3 0 0
34 17 4 1 0
34 21 11 3 1
MAPKi
Log−rank
p = 0.65
Log−rank
p = 0.68
PFS (days)
9 5 1 1 1
9 5 2 0 0
9 5 2 1 1
9 5 1 0 0
median and above
below median
G
Single cell RNA-seq (ICI)
BCR diversity, OT
BCR clonality, OT
Survival probability
Log−rank
p = 0.0041
Log−rank
p = 0.97
OS (days)
Number at risk
9 9 8 2 1 1
8 5 2 1 0 0
9 7 4 2 0 0
8 7 6 1 1 1
median and above
below median

Figure 5

A

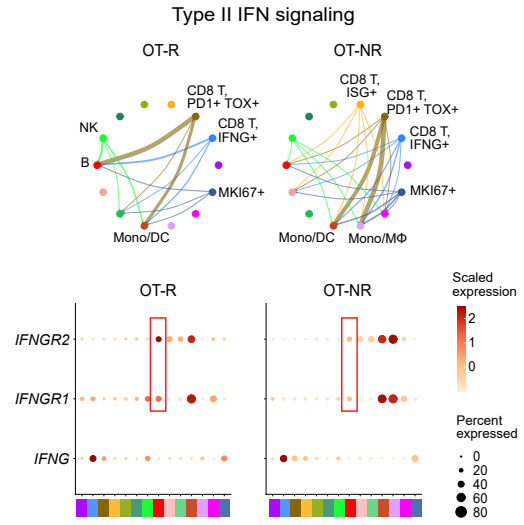

B

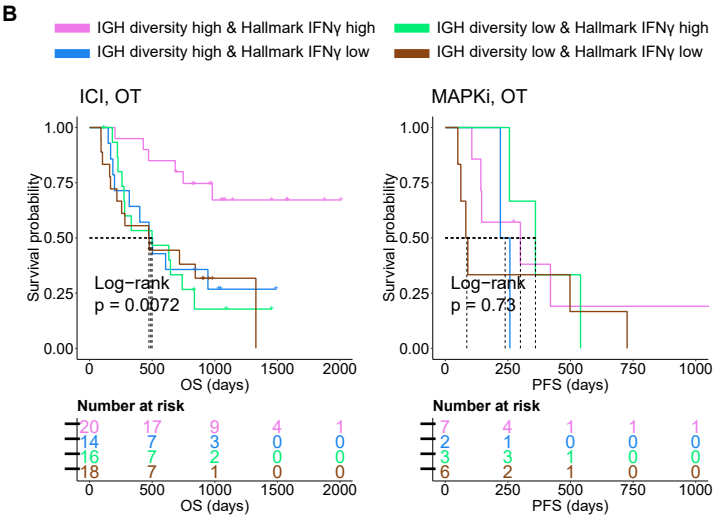

C

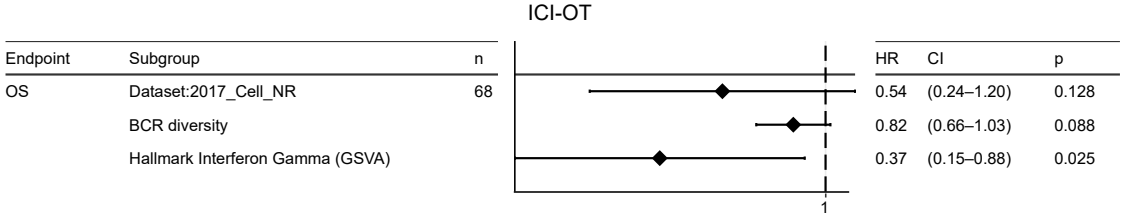

D

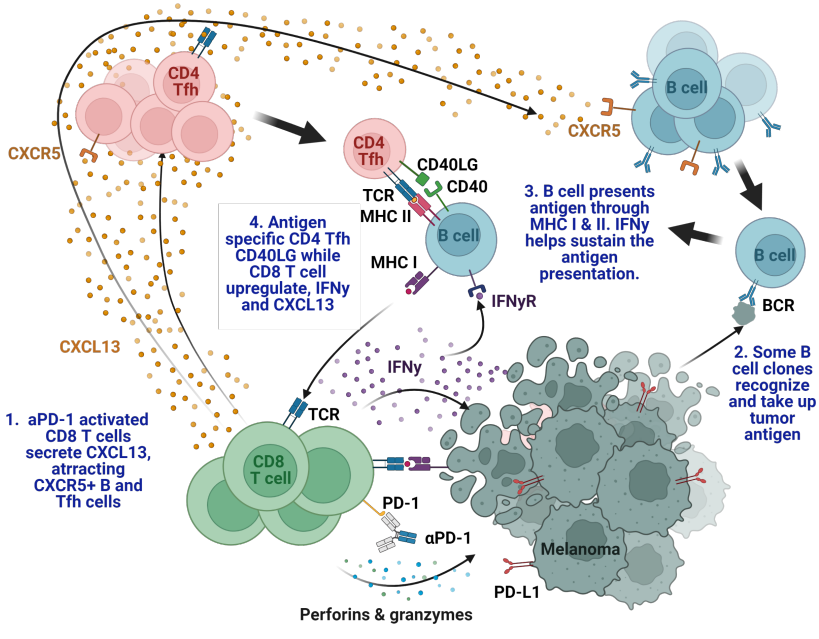

Supplementary figure 1

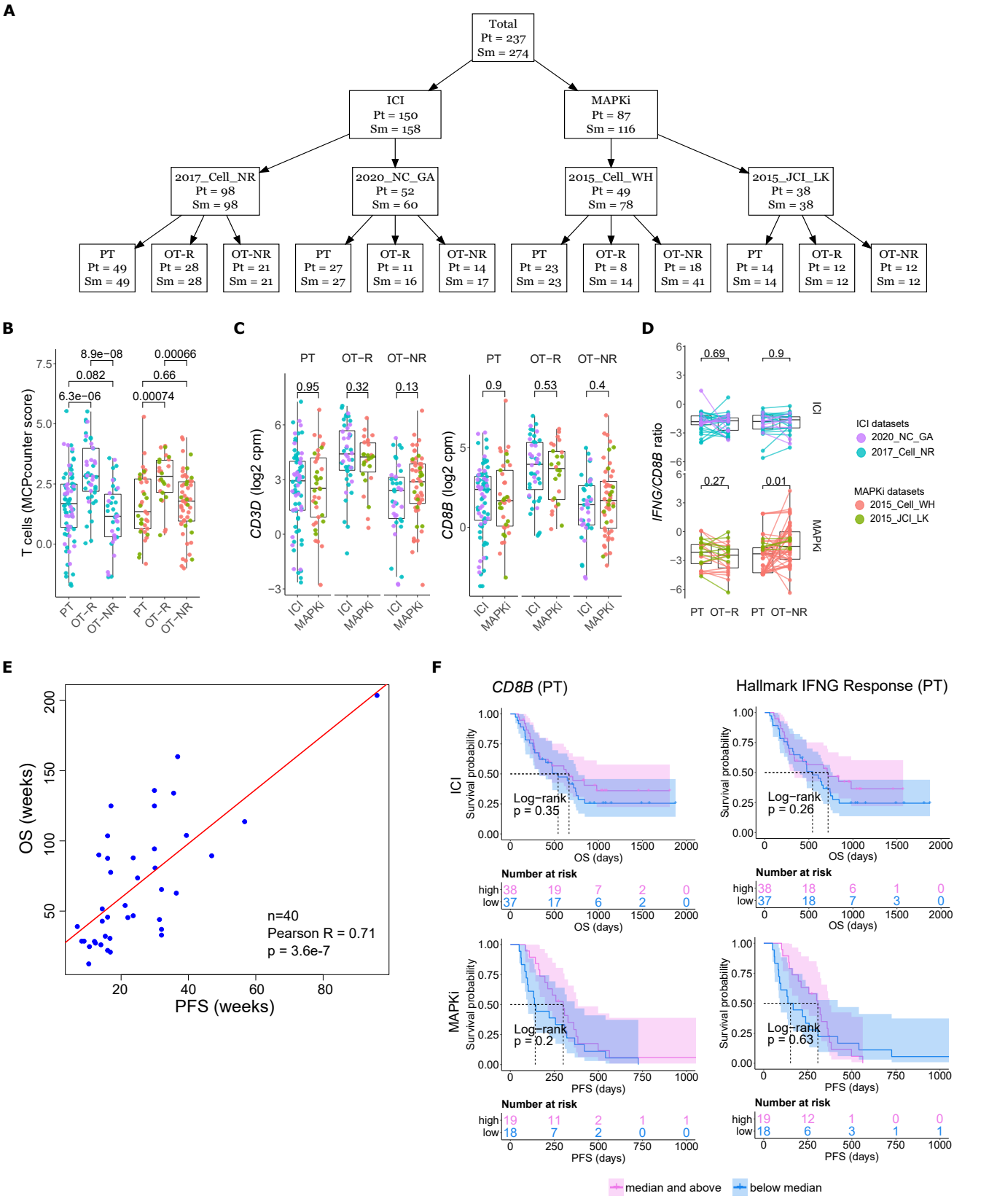

Supplementary figure 2

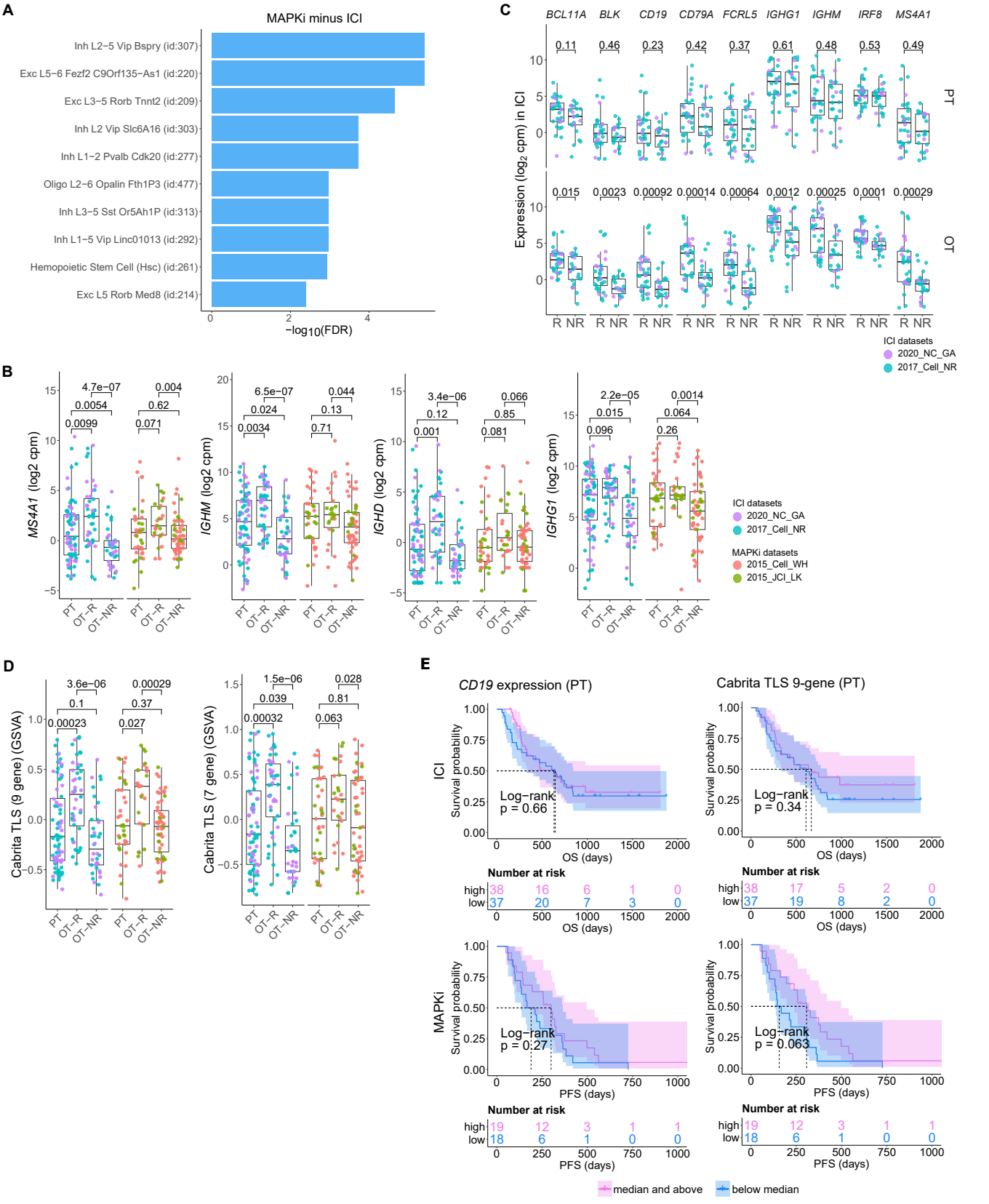

Supplementary figure 3

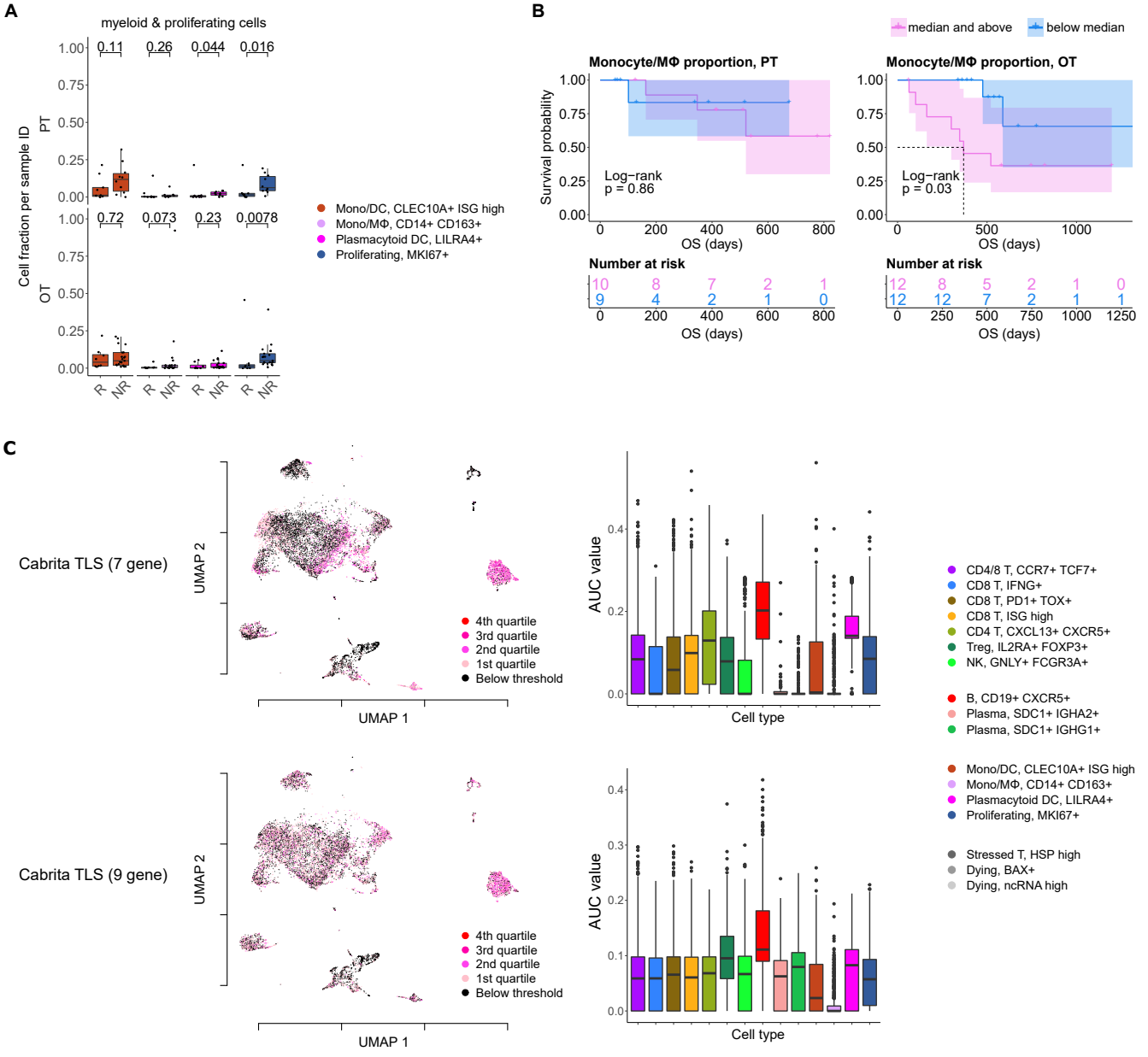

Supplementary figure 4 - part 1

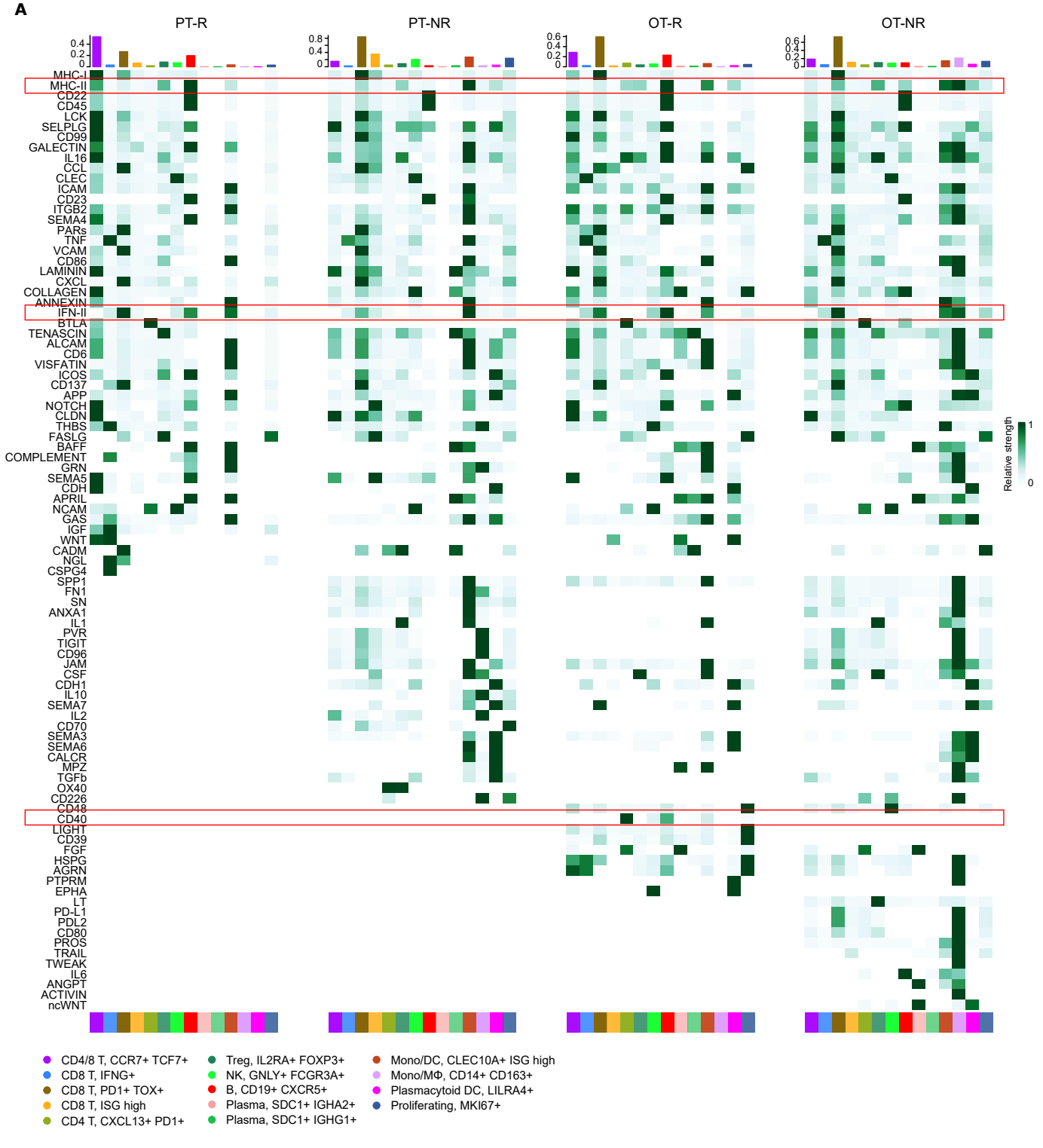

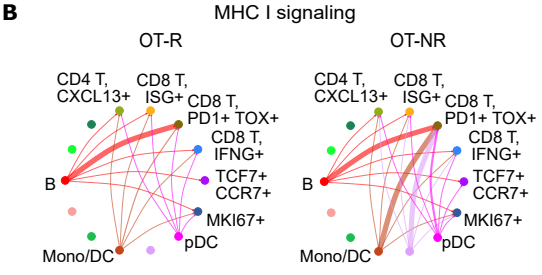

Supplementary figure 4 - part 2

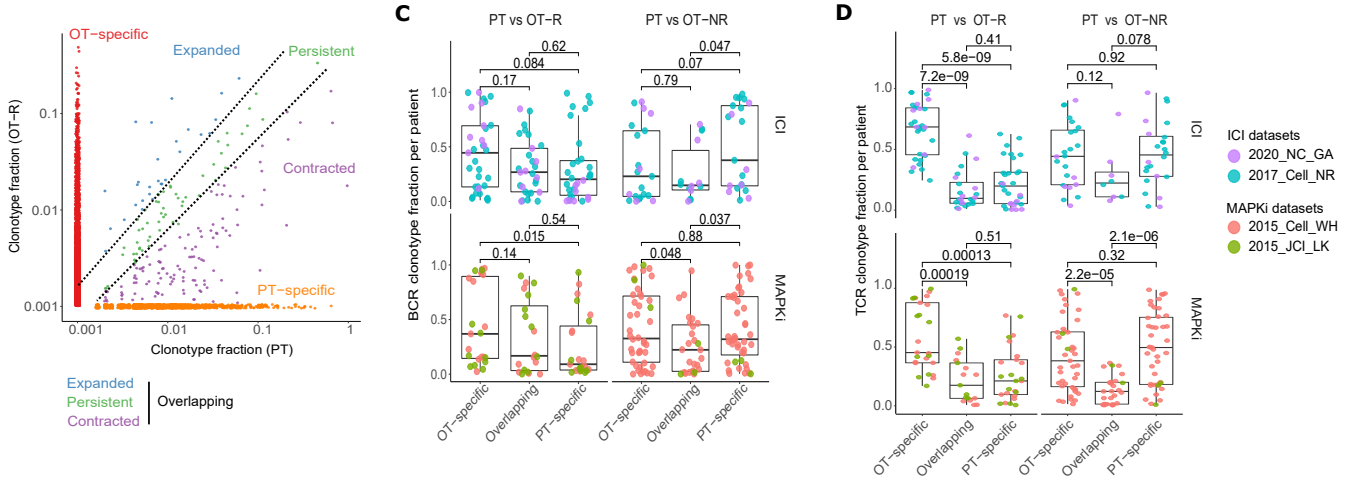

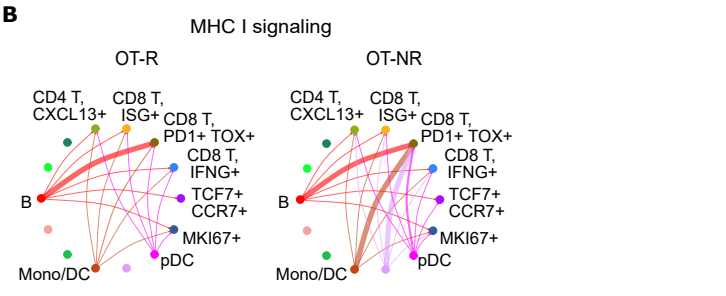

Supplementary figure 5

A

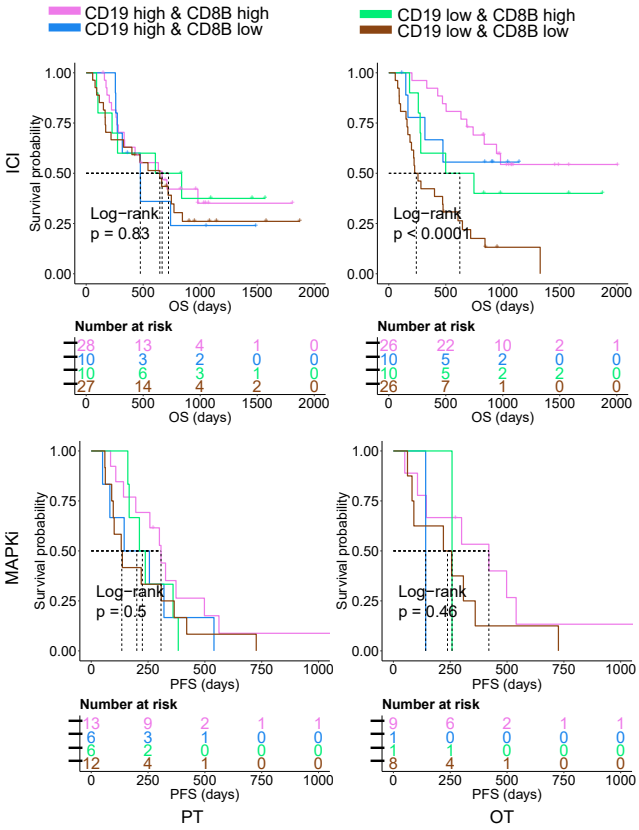

B

ICI.OT
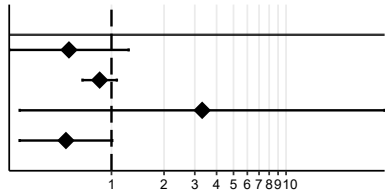
Endpoint	Subgroup	n	HR	CI	p
OS	Dataset:2017_Cell_NR	68	0.57	(0.26–1.25)	0.163
	BCR diversity		0.86	(0.68–1.07)	0.177
	Hallmark Interferon Gamma (GSVA)		3.31	(0.30–36.70)	0.330
	Interaction		0.55	(0.30–1.01)	0.054